Bull Math Biol (2019) 81:3508–3541
https://doi.org/10.1007/s11538-017-0374-2

SPECIAL ISSUE: MATHEMATICS TO SUPPORT DRUG DISCOVERY AND DEVELOPMENT

# Quantitative PET Imaging in Drug Development: Estimation of Target Occupancy

**Mika Naganawa**[1] · **Jean-Dominique Gallezot**[1] · **Samantha Rossano**[1,2] · **Richard E. Carson**[1,2]

Received: 7 August 2017 / Accepted: 27 November 2017 / Published online: 11 December 2017


**Abstract** Positron emission tomography, an imaging tool using radiolabeled tracers in humans and preclinical species, has been widely used in recent years in drug development, particularly in the central nervous system. One important goal of PET in drug development is assessing the occupancy of various molecular targets (e.g., receptors, transporters, enzymes) by exogenous drugs. The current linear mathematical approaches used to determine occupancy using PET imaging experiments are presented. These algorithms use results from multiple regions with different target content in two scans, a baseline (pre-drug) scan and a post-drug scan. New mathematical estimation approaches to determine target occupancy, using maximum likelihood, are presented. A major challenge in these methods is the proper definition of the covariance matrix of the regional binding measures, accounting for different variance of the individual regional measures and their nonzero covariance, factors that have been ignored by conventional methods. The novel methods are compared to standard methods using simulation and real human occupancy data. The simulation data showed the expected reduction in variance and bias using the proper maximum likelihood methods, when the assumptions of the estimation method matched those in simulation. Between-method differences for data from human occupancy studies were less obvious, in part due to small dataset sizes. These maximum likelihood methods form the basis for development of improved PET covariance models, in order to minimize bias and variance in PET occupancy studies.

✉ Richard E. Carson
richard.carson@yale.edu

1 PET Center, Department of Radiology and Biomedical Imaging, Yale University, 15 York Street/LMP 89A, P. O. Box 208048, New Haven, CT 06520-8048, USA

2 Department of Biomedical Engineering, Yale University, 15 York Street/LMP 89A, P. O. Box 208048, New Haven, CT 06520-8048, USA

## 1 Introduction

Drug development is lengthy, requiring 10–12 years and costing ∼1 billion USD to advance a drug to clinic (DiMasi et al. 2003). To speed and optimize this development, quantitative biomarkers are essential to demonstrate a drug's mechanism of action and ultimate utility. One very effective tool to produce relevant quantitative biomarkers is positron emission tomography (PET), a noninvasive imaging modality that provides quantitative information in vivo and can be used to assess all aspects of a drug's behavior. PET has been increasingly recognized in the pharmaceutical industry as a powerful tool that can provide essential and timely information for drug development; these applications have been particularly successful in the central nervous system (CNS) and are now spreading to other body systems. This article focuses on the use of PET for the quantitative measurement of occupancy at receptors, transporters, and enzymes, using current methods and new approaches, motivated by maximum likelihood estimation.

### 1.1 Applications of PET Imaging in CNS Drug Development

PET applications in drug development include: (1) Detection of a drug's distribution and tissue kinetics if a drug can be directly labeled; (2) Validation of target engagement by the drug to determine if the drug reaches and engages the desired target; (3) Target occupancy studies to relate a drug's dose or blood concentration to target occupancy, to determine if the drug interacts with the target at a level sufficient to produce the intended pharmacological effects; and (4) Monitoring treatment effect, to assess if the drug alters the underlying pathology. For the purposes of this manuscript, we focus on #3, measurement of target occupancy. Figure 1 shows an example of PET images measured with the kappa opioid antagonist radiotracer $^{11}$C–LY2795050 before and after an oral dose of 2 mg of LY2456302, a kappa opioid antagonist (Naganawa et al. 2016).

PET imaging for receptor occupancy studies is especially useful, as it provides the quantitative relationship of dosage with the level of target engagement. When coupled with measurement of drug concentrations in the plasma, this type of study provides information about the relationship between drug dosage, drug exposure in the circulation, occupancy of target receptor, and pharmacological response. For example, if a certain level of receptor occupancy is thought to be required for the intended efficacy, and the maximal tolerable dose (MTD) yields a lower occupancy level, clinical trials can be halted, thus saving drug development costs. Alternatively, if a specific drug has high occupancy, but does not have efficacy, this provides valuable information to develop drugs targeting other potential mechanisms.

For the CNS, brain receptor occupancy studies are typically performed first in rodents and/or nonhuman primates (NHP), and subsequently in human subjects. Examples of our own studies in NHP include occupancy at norepinephrine transporters (Gallezot et al. 2011), serotonin receptors (Cosgrove et al. 2011), dopamine receptors (Gallezot et al. 2012), acetylcholine receptors (Hillmer et al. 2016), glycine transporters (Castner et al. 2014; Xia et al. 2015), histamine receptors(Sawant-Basak et al.

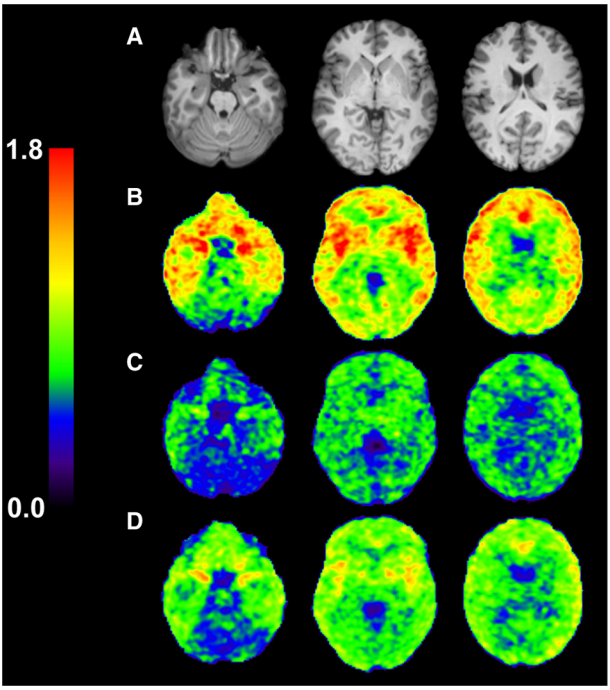


**Fig. 1** Transaxial images from a typical subject before and after an oral dose of 2 mg of LY2456302. Activity is expressed as standardized uptake values (SUVs, activity normalized by dose and body weight). MR images (**a**) and co-registered PET images summed from 30 to 90 min after injection of $^{11}$C-LY2795050 in the baseline scan (**b**), and 2 h (**c**) and 24 h (**d**) post-drug scans. High uptake is seen in the amygdala (left), insula (middle), and anterior cingulate cortex (right). The computed receptor occupancy estimated with Eq. 20 was 77% (**c**) and 58% (**d**) (Color figure online)

2017), kappa opioid receptors (Kim et al. 2013), and synaptic vesicular protein (SV2A) (Nabulsi et al. 2016; Nicolas et al. 2016). In general, we have found there to be good correlation between occupancy in NHP and occupancy in humans, after adjusting for interspecies differences in bioavailability and plasma-free fraction of drug.

As an example, consider the kappa opioid system, where a selective ligand [$^{11}$C]GR103545 was shown to be suitable for imaging this receptor in nonhuman primates (NHP) (Talbot et al. 2005). Development of this radiotracer for PET imaging in humans was carried out in our laboratory (Nabulsi et al. 2011; Naganawa et al. 2014). After validation of this radiotracer in humans, it was used in a receptor occupancy study of PF-04455254, a selective kappa antagonist. In the receptor occupancy study, PF-04455254 was given to healthy subjects at an oral dose of 30 mg and PET scans were performed at 1.5 h ($t_{max}$ for the drug) and 8 h (2 half-lives of the drug), respectively, post-dosing. Venous samples were taken during the scan to measure plasma concentrations of PF-0455254. As there is no reference region for this radiotracer (see below), the occupancy plot was used to calculate receptor occupancy (Cunningham et al. 2010). At a dose of 30 mg, mean kappa receptor occupancy of ~50%, a level expected to be useful for antidepressant efficacy. Even though the development of this

drug was halted for other reasons, the PET study with concurrent PK/PD measurements provided an important proof of mechanism study demonstrating the potential of kappa antagonists as efficacious antidepressants. Other examples of our published human occupancy studies include acetylcholine receptors (Esterlis et al. 2013), histamine receptors (Gallezot et al. 2017), kappa opioid receptors (Naganawa et al. 2016), and synaptic vesicular protein (SV2A) (Finnema et al. 2016).

### 1.2 Basics of PET Imaging

PET uses biological molecules labeled with positron-emitting radioisotopes such as carbon-11 or fluorine-18. These radiolabeled compounds (called radiotracers) are usually administered intravenously to a subject, and these molecules can then reach the target tissues and interact with a target protein in vivo. Detection occurs when the positron is emitted and annihilates with a nearby electron producing a pair of $\gamma$ rays traveling 180° apart, and coincidence detection is used to identify a "line-of-response" in which the emission occurred. Subsequently, image reconstruction algorithms estimate the 3D distribution of radioactivity concentration, with image resolution on the order of a few mm. With proper corrections for physical factors in PET (e.g., random coincidences, scatter, and deadtime), 3D images of radioactivity concentration calibrated in absolute units (Becquerels/cm$^3$, Bq/cm$^3$) are obtained. Dynamic acquisition over time produce a 4D dataset of concentration versus time, amenable to tracer kinetic modeling.

### 1.3 Quantitative Modeling Analysis of PET Data

Tracer kinetic modeling has been used for over 50 years as a tool to measure the uptake, retention, and metabolism of radiotracers (Cobelli et al. 2001). These modeling approaches depend upon the *tracer* assumption, i.e., that the mass concentration of the radiotracer is small, and thus does not alter the saturation of any enzyme or the occupancy of any receptor or transporter (e.g., radiotracer concentration $\ll K_D$, the dissociation equilibrium constant of the radiotracer). In this case, the mathematics defining the time course of the agent becomes simple, i.e., linear differential equations with constant coefficients, and compartment modeling approaches can be used (Jacquez 1985). PET tracer kinetic modeling differs from conventional whole-body compartment modeling (Li et al. 2014), which involves measurement of tracer uptake and retention in blood and urine, allowing the production of models of the uptake in various body organs, even without direct measurement of the concentration in various organs. In PET, many of the equations are similar, but the structure of the model differs. Since the PET system measures the activity *in* the target organ of interest over time, for organs where delivery of tracer can only occur from arterial blood and clearance can only occur via venous blood, i.e., excluding liver and lungs, we avoid the need for knowledge about the rest of the body by measuring (or inferring) the concentration of the tracer in the plasma. The time course of radiotracer in plasma is the input function to the target organ. With the input function and each tissue's time-activity curve (TAC), various compartment models are derived which can best fit the dynamic data (Carson

2003). Due to limits in precision of reconstructed PET data, these models typically contain 1 or 2 tissue compartments.

In addition, other simplified or graphical methods have been extensively used to extract a subset of model parameters, without definition of a specific model configuration (Ichise et al. 2002; Logan et al. 1990b). Another significant development was various methods to infer the input function, by use of the TAC in a "reference region," i.e., a region with no specific binding of the radiotracer (Ichise et al. 2003; Lammertsma and Hume 1996; Logan et al. 1996). This approach has been most widely used in the brain using agents targeted at one neurotransmitter system where there are regions of the brain completely or nearly devoid of this receptor. Once validated, this approach obviates the need for measurements of the input function that, in principle, should be acquired from arterial blood. A further complication of input function measurements is that the radioactivity in circulation is a combination of the original injected tracer (the parent compound), plus radiolabeled metabolites produced by the body; this requires correction of the radioactivity measurements for these radiolabeled metabolites.

### 1.4 Quantification of Receptor Occupancy

For radiotracers designed to bind to protein targets such as receptors, transporters, or enzymes, the PET modeling community adopted nomenclature for the quantitative outcome measures derived from kinetic analyses (Innis et al. 2007). For the purposes of this text, we will use the word "receptor" for the protein target. The two key measures are the volume of distribution ($V_T$) and the binding potential ($BP$). $V_T$ is the equilibrium ratio of the tissue to plasma; this ratio reflects the radiotracer that is specifically bound to the receptor, as well as free or nonspecifically bound (the latter two components termed "nondisplaceable" since competing agents do not displace this component of the tracer uptake). Mathematically,

$$V_T = V_{ND} + V_S \tag{1}$$

where the subscripts T, ND, and S, refer to total, nondisplaceable, and specific, respectively. Most PET studies use bolus injection of a radiotracer, so the modeling estimates the equilibrium ratio by estimating $V_T$ from the kinetic parameters determined from a model fit to the dynamic data [unless constant infusion is used to reach equilibrium conditions (Carson et al. 1993)].

The binding potential, $BP$, is an equilibrium ratio of the concentration of specifically bound tracer to that in a reference fluid or region. Three versions of $BP$ are used, using 3 different references: free radiotracer in plasma ($BP_F$), total in plasma ($BP_P$), or the tissue nondisplaceable component ($BP_{ND}$). $BP_{ND}$ ($V_S/V_{ND}$) is most commonly used, since this term can be estimated using the reference region methods. The primary assumption of reference regions is that the $V_T$ in the reference region (REF) is equal to $V_{ND}$ in the target region-of-interest (ROI). When calculated from $V_T$, $BP_{ND}$ is

$$BP_{ND} = \frac{V_{T,ROI} - V_{T,REF}}{V_{T,REF}} = \frac{V_S}{V_{ND}} \tag{2}$$

Receptor occupancy ($r$) of a drug candidate at a target can then be measured quantitatively if the drug and the tracer bind to the same receptor. This is typically performed by using 2 PET scans in the same subject, one at baseline (base), and one at a suitable time post-administration of a drug of interest (post). $V_T$ is reduced in the post-drug scan due to drug occupancy and reduction of specific binding. Assuming there is no change in nondisplaceable binding induced by the drug:

$$V_T = V_{ND} + (1 - r)V_S \tag{3}$$

If a reference region is available, the binding potential in the post-drug scan is:

$$BP_{ND,post} = \frac{V_{ND} + (1 - r)\, V_{S,ROI} - V_{T,REF}}{V_{T,REF}} \tag{4}$$

and $r$ can be determined independently for each ROI

$$r = \frac{BP_{ND,base} - BP_{ND,post}}{BP_{ND,base}} \tag{5}$$

Alternatively, if there is no suitable reference region devoid of receptors, $r$ can be determined without a reference region from $V_T$ values from multiple regions using the "occupancy plot" under the assumptions that $r$ and nondisplaceable binding ($V_{ND}$) are uniform across brain regions (Cunningham et al. 2010). This commonly used method is not statistically optimal (as detailed in Sect. 3.1.1), and development and evaluation of alternative methods is the topic of this manuscript.

Ultimately, $r$ values can be compared to the dose of the drug ($D$) or the plasma concentration ($C$) of the drug to estimate the $ID_{50}$ or $IC_{50}$, the dose or concentration that produces 50% occupancy of the target. This analysis is typically done by combining data from multiple subjects or from having multiple post-drug scans (at different doses or plasma drug levels) in one subject.

### 1.5 Scope of this Presentation

In this presentation, we focus on estimating receptor occupancy ($r$) from a single subject. This is typically based on 2 scans (baseline and post-drug), but we also include 3-scan paradigms (baseline plus 2 post-drug scans), estimating 2 occupancy values ($r_1$, $r_2$). In addition, since many tracers have no ideal reference region, here we consider only those tracers, i.e., where nondisplaceable binding levels ($V_{ND}$) must also be estimated from multi-region data.

In the discussion, we consider other paradigms for occupancy measurements. These include multiple subject analysis (to permit $IC_{50}$ or $ID_{50}$ estimation), analyses where reference regions are available, or methods to be used when there is no baseline scan available.

Our goal is to devise new methods that produce estimates of occupancy with better accuracy and/or precision than the current approaches. We do this first with simulation, where there is a ground truth, in order to directly assess any advantages of the new

methods. However, such simulations require assumptions, which may not be met in the case of real data, or may be met to different degrees for different tracers. Therefore, we subsequently compare the methods in 3 real-data cases, in order to assess whether the same patterns are found as in the simulation, recognizing that there is no ground truth in these cases.

## 2 $V_T$ Estimation and Noise Models

### 2.1 Compartment and Graphical Methods to Measure $V_T$

By definition, the volume of distribution $V_T$ is the ratio of the tracer concentration in the tissue ($C_T$) and in the arterial plasma ($C_a$) at equilibrium. One of the simplest methods to estimate volumes of distribution is equilibrium analysis (EA), where the tracer is continuously infused until constant concentrations (i.e., equilibrium) are obtained in plasma and all target tissues; here we ignore radioactive decay. In practice, a bolus plus infusion is used in an attempt to reach equilibrium within a practical study duration (Carson 2000). In a bolus plus infusion protocol, an initial short bolus of tracer is injected first (worth $K_{bol}$ minutes of infusion), and the rest of the tracer is infused uniformly over time. Selecting the right $K_{bol}$ value is critical for the success of a bolus plus infusion study. However, such a protocol is not always possible (1) if the time to reach equilibrium is too long, (2) if different tissues (including plasma) have very different clearance rates and therefore require different $K_{bol}$ values to reach a constant concentration quickly, or (3) if there is too much variability in the optimal $K_{bol}$ value across subjects.

Another way to estimate volumes of distributions is to use a compartment model following a bolus intravenous injection of tracer to fit tissue curves, using the measured input function in plasma. For a review of commonly used compartment models in PET, see (Gunn et al. 2001). The operational equations of compartmental models can always be written as:

$$\widehat{C_T}(t) = C_a(t) \otimes h(t) \tag{6}$$

where $\otimes$ is the convolution operator and $h(t)$ is the tissue impulse response function, i.e., a sum of $n$ exponential functions, $n$ being the number of compartments in the model. To determine the best way to quantify a new tracer, various compartment models are tested and compared, to determine the simplest model that accurately fits the TACs, while providing stable $V_T$ estimates. In practice, a few reversible PET tracers can be accurately modeled using the one-tissue compartment (1TC) model, which requires estimating only two parameters, the influx rate constant $K_1$ and the efflux rate constant $k_2$. The volume of distribution $V_T$ is then equal to the ratio of $K_1$ and $k_2$. The other reversible tracers can usually be accurately modeled using the two-tissue compartment (2TC) model, which requires estimating four parameters: the influx rate constant $K_1$, the first-compartment efflux rate constant $k_2$, the transfer rate constant $k_3$ from the first to the second compartment, and its reciprocal $k_4$. The volume of distribution $V_T$ is then equal to $K_1/k_2 \times (1 + k_3/k_4)$. For the 2TC model, it is in

general difficult to obtain reliable estimates of $k_2$, $k_3$ and $k_4$, but reliable estimates of $K_1$ and $V_T$ can be obtained for many tracers.

A third way to estimate volumes of distributions is to use so-called graphical analysis (Logan et al. 1990a), in which a plot of $\int_0^t C_T(\tau)\,d\tau / C_T(t)$ versus $\int_0^t C_a(\tau)\,d\tau / C_T(t)$ is created. Such a plot is asymptotically linear, and the asymptotic slope is equal to $V_T$. This method is general in the sense that it can theoretically be used for any reversible compartment model, whatever the number and arrangement of the compartments. However, this method has two drawbacks. First, it requires selecting a time $t^*$ after which the plot is considered linear. Second, this method can be highly biased when there is noise in the tissue curve (Slifstein and Laruelle 2000). Several methods have been derived from the original graphical analysis to reduce this noise-induced bias, such as multilinear analysis one (MA1) (Ichise et al. 2002) and likelihood estimation in graphical analysis (LEGA) (Ogden 2003). The MA1 operational equation is:

$$\widehat{C_T}(t) = -\frac{V_T}{b}\int_0^t C_a(\tau)\,d\tau + \frac{1}{b}\int_0^t C_T(\tau)\,d\tau,\ t > t^* \tag{7}$$

where the parameter $b$ is the intercept of the asymptotic line in the graphical analysis. The LEGA operational equation is recursive and can be written as:

$$\widehat{C_T}(t_i) = \frac{\sum_{f=0}^{i-1}\widehat{C_T}(t_f)\left(S_f - S_{f-1}\right) + \frac{1}{8}\widehat{C_T}(t_{i-1})\left(S_i - S_{i-1}\right) - b \times \int_0^{t_i}\widehat{C_a}(\tau)\,d\tau}{V_T - \frac{3}{8}\left(S_i - S_{i-1}\right)},\ t > t^* \tag{8}$$

where $t_i$ and $S_i$ are the mid- and end times of PET frame number $i$, and $\widehat{C_T}(t_{i-1}) = C_T(t_{i-1})$ if $t_i$ is the first frame after $t^*$.

In practice, MA1 and LEGA $V_T$ estimates are often less variable than 2TC $V_T$ estimates, since those two methods only require estimating 2 parameters. While they are less biased than Logan graphical analysis, some bias may remain depending on the selection of the time $t^*$.

Among the aforementioned methods, EA uses a linear estimator for $V_T$; MA1 is bilinear, but $V_T$ is not one of the linear parameters, so it is obtained as a function of the two linear parameters; and LEGA and compartmental model parameters are obtained using nonlinear weighted least square estimation.

### 2.2 Noise Models for $V_T$

Noise in dynamic PET data and noise in the input function data will lead to noise in the $V_T$ estimates. Although the count data on which PET images are based are Poisson in nature, the process of PET image reconstruction and the subsequent PET data processing to determine $V_T$ can add additional noise sources, as well as altering the distribution of the noise. Part of this noise is independent across ROIs (e.g., local image noise due to counting statistics), while part of this noise is not independent across ROIs (e.g., calibration errors, noise in the input function, ROI-delineation errors due to coregistration errors between PET and MR images).

Local image noise due to counting statistics is often assumed to have a variance proportional to the mean of counts. The resulting variance of an ROI TAC $C_{\mathrm{T}}(t)$ is then modeled as follows:

$$\sigma^2_{C_{\mathrm{T}}} = \alpha \frac{C_{\mathrm{T}}(t) \times 2^{t/t_{1/2}}}{\Delta t} \tag{9}$$

where $t_{1/2}$ is the half-life of the tracer's isotope, $\Delta t$ is the frame duration at time $t$, and $\alpha$ is a scaling factor. If $C_{\mathrm{T}}(t)$ is expressed in radioactivity units (e.g., Bq/mL), then $\alpha$ is independent of the injected dose. However, $\alpha$ is also a (decreasing) function of the ROI size. If all voxels in the ROI were statistically independent, $\alpha$ would be proportional to $1/n$, where $n$ is the number of voxels in the ROI. A practical way to estimate $\alpha$ is to use the residual sum of squares from weighted fits of ROI data with the following formula:

$$\alpha = \mathrm{WRSS}/n_{\mathrm{f}} \tag{10}$$

where WRSS is the weighted residual sum of squares and $n_{\mathrm{f}}$ is number of degrees of freedom of the fit. The weights used for these fits should be the inverse of the variances above, excluding $\alpha$:

$$W(t) = \frac{\Delta t}{C_{\mathrm{T}}(t)} \times 2^{-t/t_{1/2}} \tag{11}$$

If $V_{\mathrm{T}}$ is estimated using a linear estimator (i.e., $\boldsymbol{Y} = \boldsymbol{X}\boldsymbol{\beta}$, where $\boldsymbol{Y}$ is the vector of observed PET data, $\boldsymbol{\beta}$ are the parameters, and $\boldsymbol{X}$ is the matrix with columns that are the independent variables), noise in each $C_{\mathrm{T}}$ value is assumed to be Gaussian and independent, and the variance is assumed to be known up to a scale factor. Then, the theoretical covariance matrix of the estimated parameters is:

$$\mathbf{cov}_{\boldsymbol{\beta}_{\mathrm{ML}}} = s^2 \left( \boldsymbol{X}^{\mathrm{T}} \boldsymbol{\Sigma}^{-1} \boldsymbol{X} \right)^{-1} \tag{12}$$

where $s^2 = \frac{1}{n_{\mathrm{f}}} (\boldsymbol{Y} - \boldsymbol{Y})^{\mathrm{T}} \boldsymbol{\Sigma}^{-1} (\boldsymbol{Y} - \boldsymbol{Y})$ is the residual sum of weighted residuals normalized by the number of degrees of freedom, $\boldsymbol{\Sigma}$ is the (assumed) covariance matrix of the noise in the PET data. If $\boldsymbol{\Sigma}$ is scaled correctly, then the term $s^2$ equals one.

If $V_{\mathrm{T}}$ is estimated using a nonlinear estimator (e.g., using a compartmental model) with weighted least squares, and the variance of the noise in the PET data is assumed to be known up to a scale factor, then the theoretical covariance matrix of the estimated parameters is an approximation, also given by Eq. (12), where $\boldsymbol{X}$ is the sensitivity matrix with columns that are the partial derivative of the model function with respect to each parameter.

If $V_{\mathrm{T}}$ is one of the model parameters, then the theoretical standard error of $V_{\mathrm{T}}$ can be extracted directly from the relevant diagonal element of $\mathbf{cov}_{\boldsymbol{\beta}_{\mathrm{ML}}}$. If $V_{\mathrm{T}}$ is not one of the fitted model parameters, then the standard error can be estimated using $\mathbf{cov}_{\boldsymbol{\beta}_{\mathrm{ML}}}$ and the error propagation equation:

$$\sigma^2_{f(x,y)} = \sigma^2_x \left( \frac{\partial f}{\partial x} \right)^2 + \sigma^2_y \left( \frac{\partial f}{\partial y} \right)^2 + 2\sigma^2_{x,y} \left( \frac{\partial f}{\partial x} \frac{\partial f}{\partial y} \right) \tag{13}$$

where $\sigma^2_x$ and $\sigma^2_{x,y}$ are diagonal and off-diagonal elements of $\mathbf{cov}_{\boldsymbol{\beta}_{\mathrm{ML}}}$, respectively

### 2.3 Covariance Models for Multi-region $V_T$

If the statistical noise in each ROI TAC is assumed to be independent from the noise in other ROIs, and the noise in the input function is ignored, then the noise in estimated regional $V_T$ values will be independent. However, when the noise in the input function is not negligible, ROI $V_T$ values from the same scan will be correlated.

As an approximation, assuming that EA is used to estimate $V_T$ as $C_T/C_a$, then using the error propagation equation, the diagonal elements of the covariance matrix of regional $V_T$ estimates can be expressed as:

$$\begin{aligned}\sigma^2_{V_{T,i}} &= \sigma^2_{C_{T,i}}\left(\frac{\partial V_{T,i}}{\partial C_{T,i}}\right)^2 + \sigma^2_{C_a}\left(\frac{\partial V_{T,i}}{\partial C_a}\right)^2 = \sigma^2_{C_{T,i}}\left(\frac{1}{C_a}\right)^2 + \sigma^2_{C_a}\left(\frac{C_{T,i}}{C_a^2}\right)^2 \\ &= \frac{\sigma^2_{C_{T,i}} + \sigma^2_{C_a} V^2_{T,i}}{C_a^2} \end{aligned} \tag{14}$$

where $V_{T,i}$ is the estimated $V_T$ in ROI $i$, $C_{T,i}$ is the tissue concentration at equilibrium in ROI $i$, and $C_a$ is the plasma concentration at equilibrium and $\sigma^2_{C_{T,i}}$ and $\sigma^2_{C_a}$ are the variances of $C_{T,i}$ and $C_a$, respectively. Similarly, the off-diagonal elements of the $V_T$ covariance matrix are:

$$\sigma^2_{V_{T,i},V_{T,j}} = \sigma^2_{C_a}\frac{\partial V_{T,i}}{\partial C_a}\frac{\partial V_{T,j}}{\partial C_a} = \sigma^2_{C_a}\frac{C_{T,i}}{C_a^2}\frac{C_{T,j}}{C_a^2} = \frac{\sigma^2_{C_a}}{C_a^2} V_{T,i} V_{T,j} \tag{15}$$

When a compartmental model is used to estimate $V_T$, no such simple formula is available. Previous evaluation of the impact of the noise in the input function can be found in (Chen et al. 1991; Huesman and Mazoyer 1987; Normandin et al. 2012). In this study, we used the following model, inspired by Eqs. (14) and (15):

$$V_{T,\text{noisy}} = V_{T,\text{truth}}\,(1 + \epsilon_{\text{aif}}) + \epsilon_{V_{T,i}} \tag{16}$$

where $\epsilon_{\text{aif}}$ and $\epsilon_{V_{T,i}}$ are Gaussian random variables with zero mean and "aif" refers to the arterial input function. The variance of $\epsilon_{V_{T,i}}$ (denoted $\sigma^2_{V_{T,i},\text{no input noise}}$) was evaluated based on the noise in PET TACs using equations in Sect. 2.2. The standard deviation of $\epsilon_{\text{aif}}$ (denoted $\sigma_{\text{aif}}$) contributes to the covariance matrix of $V_T$ according to the following equations:

$$\sigma^2_{V_{T,i}} = \sigma^2_{V_{T,i},\text{no input noise}} + \sigma^2_{\text{aif}} V^2_{T,i} \tag{17}$$

$$\sigma^2_{V_{T,i},V_{T,j}} = \sigma^2_{\text{aif}} V_{T,i} V_{T,j} \tag{18}$$

which provide the diagonal and off-diagonal terms, respectively. Using real PET study data, $\sigma_{\text{aif}}$ was evaluated from test/retest studies (Naganawa et al. 2015), i.e., 2 back-to-back scans in the same subject. The term $\sigma_{\text{aif}}$ is then calculated using the excess variability between test and retest $V_T$ estimates not explained by $\sigma^2_{V_{T,i},\text{no input noise}}$, using the following equation:

$$\sigma^2_{V_{\mathrm{T},i,\mathrm{diff}}} = 2\sigma^2_{V_{\mathrm{T},i,\text{no input noise}}} + 2\sigma^2_{\mathrm{aif}} V^2_{\mathrm{T},i} \tag{19}$$

where $\sigma^2_{V_{\mathrm{T},i,\mathrm{diff}}}$ is the standard deviation of the difference between test and retest $V_\mathrm{T}$ values (i.e., $V_{\mathrm{T},i,\mathrm{diff}} = V_{\mathrm{T},i,\mathrm{retest}} - V_{\mathrm{T},i,\mathrm{test}}$).

## 3 Methods to Estimate Occupancy Without a Reference Region

### 3.1 One Post-Drug Scan

#### *3.1.1 Standard Occupancy Plot (OCCPLOT)*

The standard occupancy plot (Cunningham et al. 2010) is derived from equations for $V_\mathrm{T}$ [Eqs. (1), (3)]. Assuming that $V_\mathrm{ND}$ and $r$ are the same for all regions, the occupancy plot can be described as:

$$\boldsymbol{V}_{\mathrm{T,base}} - \boldsymbol{V}_{\mathrm{T,post}} = r\left(\boldsymbol{V}_{\mathrm{T,base}} - V_\mathrm{ND}\boldsymbol{u}\right) \tag{20}$$

where $\boldsymbol{V}_{\mathrm{T,base}}$ and $\boldsymbol{V}_{\mathrm{T,post}}$ are column vectors of the distribution volumes from $n$ regions at baseline and post-drug administration, respectively, and $\boldsymbol{u}$ is a column $n$-vector of ones. Plotting $\boldsymbol{V}_{\mathrm{T,base}} - \boldsymbol{V}_{\mathrm{T,post}}$ (on the $y$-axis) against $\boldsymbol{V}_{\mathrm{T,base}}$ (on the $x$-axis) across $n$ regions leads to a linear relationship with a slope equal to $r$ and $x$ intercept equal to $V_\mathrm{ND}$. In PET studies, an unweighted linear least squares estimator is commonly used to estimate the slope and $y$ intercept. $V_\mathrm{ND}$ is obtained as $-(y\text{intercept})\,/\,r$. This method is frequently used because of easy visualization; however, it violates the assumptions of ordinary least squares estimation since (1) the independent variable, $V_{\mathrm{T,base}}$ is noisy, (2) that noise is correlated with the dependent variables, and (3) the dependent variables are not independent. Further, if the standard error of $r$ is calculated from this plot applying the incorrect OLS assumptions, this standard error may be inaccurate, due to the violation of these assumptions.

#### *3.1.2 Maximum Likelihood (ML) Estimation*

The measured $V_\mathrm{T}$ values of the $i$th ROI at baseline and post-drug administration are modeled as:

$$V_{\mathrm{T,base},i} = V_\mathrm{ND} + V_{\mathrm{S},i} + \varepsilon_i \tag{21}$$

$$V_{\mathrm{T,post},i} = V_\mathrm{ND} + (1-r)\,V_{\mathrm{S},i} + \varepsilon_i \tag{22}$$

where $\varepsilon_i$ is additive Gaussian noise.

Let $\boldsymbol{\theta} = \left[V_{\mathrm{S},1}, V_{\mathrm{S},2}, \ldots, V_{\mathrm{S},n}, V_\mathrm{ND}, r\right]$ be the vector of parameters to estimate. The elements of $\boldsymbol{\theta}$ are estimated by minimizing the cost function:

$$g\left(\boldsymbol{\theta}\right) = \left(\boldsymbol{v}_\mathrm{T} - \boldsymbol{f}\left(\boldsymbol{\theta}\right)\right)^\mathrm{T} \boldsymbol{\Sigma}^{-1} \left(\boldsymbol{v}_\mathrm{T} - \boldsymbol{f}\left(\boldsymbol{\theta}\right)\right) \tag{23}$$

where $\boldsymbol{v}_{\mathrm{T}}$ is a vector of the measured distribution volumes at baseline and post-drug administration ($2n$ values) and $\boldsymbol{\Sigma}$ is the $2n$-by-$2n$ data covariance matrix. $\boldsymbol{f}(\boldsymbol{\theta})$ is the model function as shown in Eqs. (21) and (22).

Since the covariance matrix is a real symmetric matrix, it can be eigendecomposed as $\boldsymbol{\Sigma} = \boldsymbol{Q}\boldsymbol{\Lambda}\boldsymbol{Q}^{\mathrm{T}}$ where $\boldsymbol{Q}$ is the square matrix of eigenvectors $(\boldsymbol{e}_1, \boldsymbol{e}_2, \ldots, \boldsymbol{e}_{2n})$ and $\boldsymbol{\Lambda}$ is a diagonal matrix whose diagonal elements are the corresponding eigenvalues $(\lambda_1, \lambda_2, \ldots, \lambda_{2n})$. Equation (23) is rewritten as:

$$g(\boldsymbol{\theta}) = (\boldsymbol{v}_{\mathrm{T}} - \boldsymbol{f}(\boldsymbol{\theta}))^{\mathrm{T}} \boldsymbol{Q}\boldsymbol{\Lambda}^{-1}\boldsymbol{Q}^{\mathrm{T}} (\boldsymbol{v}_{\mathrm{T}} - \boldsymbol{f}(\boldsymbol{\theta})) = \sum_{i=1}^{2n} \frac{1}{\lambda_i} \left( (\boldsymbol{v}_{\mathrm{T}} - \boldsymbol{f}(\boldsymbol{\theta}))^{\mathrm{T}} \boldsymbol{e}_i \right)^2 \quad (24)$$

If we have no prior knowledge of the noise covariance matrix and uniform variance in all $V_{\mathrm{T}}$ values is assumed, the data covariance matrix is of the form, $\boldsymbol{\Sigma} = \sigma^2 \boldsymbol{I}$, where $\boldsymbol{I}$ is the identity matrix. In this case, it is also assumed that the noise is uncorrelated across regions and across scans and identically distributed with a common variance $\sigma^2$. Therefore, the cost function is reduced to the following equation.

$$g(\boldsymbol{\theta}) = \frac{1}{\sigma^2} \left( \sum_{i=1}^{n} \left( V_{\mathrm{T,base},i} - V_{\mathrm{S},i} - V_{\mathrm{ND}} \right)^2 + \sum_{i=1}^{n} \left( V_{\mathrm{T,post},i} - (1-r) V_{\mathrm{S},i} - V_{\mathrm{ND}} \right)^2 \right) \quad (25)$$

The parameters can be estimated using ordinary least squares (OLS) method. We will refer to this method as ML-OLS.

As described in Sect. 2, it is natural to introduce different noise variances between regions and scans, i.e., $\boldsymbol{\Sigma}$ is a diagonal matrix with nonconstant variance. The cost function can be written as follows:

$$g(\boldsymbol{\theta}) = \sum_{i=1}^{n} \frac{1}{\sigma^2_{\mathrm{base},i}} \left( V_{\mathrm{T,base},i} - V_{\mathrm{S},i} - V_{\mathrm{ND}} \right)^2 + \sum_{i=1}^{n} \frac{1}{\sigma^2_{\mathrm{post},i}} \left( V_{\mathrm{T,post},i} - (1-r) V_{\mathrm{S},i} - V_{\mathrm{ND}} \right)^2 \quad (26)$$

where $\sigma^2_{(\mathrm{base|post}),i}$ denotes the noise variance of $i$th region at baseline or post-drug administration. The parameters can be estimated using weighted least squares (WLS) method. The weights are the inverse of the noise variances. We will refer to this method as ML-WLS.

If the $V_{\mathrm{T}}$ values are assumed to be correlated, both within and between scans, the off-diagonal terms of the covariance matrix cannot be ignored. In this case, the parameters can be estimated by minimizing the cost function [Eq. (24)] using WLS method by transforming the $V_{\mathrm{T}}$ and $\boldsymbol{f}(\boldsymbol{\theta})$ data vectors by the matrix $\boldsymbol{Q}$ and using weights equal to the inverse of the eigenvalues. Since this approach uses the full covariance matrix, we will refer to it as ML-FCM.

### 3.2 Multiple Post-Drug Scans

#### *3.2.1 Simultaneous Occupancy Plot Estimation (OCCPLOT2)*

More than one post-drug scans are sometimes acquired in the same subject, e.g., by performing one post-drug scan at peak plasma concentration and a second post-drug scan at a later time. Consider the case of one scan at baseline and $m$ post-drug scans. The simplest approach is to apply the occupancy plot [Eq. (20)] sequentially to the baseline scan and the $k$th post-drug scan to obtain $m$ occupancy values and $m V_{\mathrm{ND}}$ values. However, $V_{\mathrm{ND}}$ can be assumed to be constant across these scans. Assuming that $V_{\mathrm{ND}}$ is the same for all scans, the cost function can be written as:

$$g\left(\boldsymbol{\theta}\right) = \sum_{k=1}^{m}\sum_{i=1}^{n}\left(V_{\mathrm{T,base,i}} - V_{\mathrm{T,post,i,k}} - \left(V_{\mathrm{T,post,i,k}} - V_{\mathrm{ND}}\right) r_k\right)^2 \tag{27}$$

where $V_{\mathrm{T,post,i,k}}$ denotes the distribution volume of the $i$th region at the $k$th post-drug administration. The elements of the $(m + 1)$ parameter vector $\boldsymbol{\theta} = [V_{\mathrm{ND}}, r_1, r_2, \ldots, r_m]$ and are estimated using OLS.

#### *3.2.2 Maximum Likelihood Estimation for Multiple Post-Drug Scans*

In case of more than one post-drug scan, Eq. (25) can be extended as (ML-OLS2):

$$\begin{aligned} g\left(\boldsymbol{\theta}\right) = \frac{1}{\sigma^2}\Bigg(&\sum_{i=1}^{n}\left(V_{\mathrm{T,base},i} - V_{\mathrm{S},i} - V_{\mathrm{ND}}\right)^2 \\ &+ \sum_{k=1}^{m}\sum_{i=1}^{n}\left(V_{\mathrm{T,post,i,k}} - \left(1 - r_k\right) V_{\mathrm{S,i}} - V_{\mathrm{ND}}\right)^2\Bigg) \end{aligned} \tag{28}$$

Equation (26) is also extended in a similar way (ML-WLS2)

$$\begin{aligned} g\left(\boldsymbol{\theta}\right) = &\sum_{i=1}^{n}\frac{1}{\sigma^2_{\mathrm{base},i}}\left(V_{\mathrm{T,base},i} - V_{\mathrm{S},i} - V_{\mathrm{ND}}\right)^2 \\ &+ \sum_{k=1}^{m}\sum_{i=1}^{n}\frac{1}{\sigma^2_{\mathrm{post},i,k}}\left(V_{\mathrm{T,post,i,k}} - \left(1 - r_k\right) V_{\mathrm{S,i}} - V_{\mathrm{ND}}\right)^2 \end{aligned} \tag{29}$$

where $\sigma^2_{\mathrm{post},i,k}$ denotes the noise variance of $i$th region at the $k$th post-drug scan.

Lastly, if we know the full covariance matrix, let $v_{\mathrm{T}}$ be a $n$-by-$(m+1)$ vector of the distribution volumes at baseline and $m$ post-drug scans and $\boldsymbol{f}$ be the corresponding model vector. The cost function [Eq. (24)] is extended as (ML-FCM2):

$$g(\boldsymbol{\theta}) = (\boldsymbol{v}_{\mathrm{T}} - \boldsymbol{f}(\boldsymbol{\theta}))^{\mathrm{T}} \mathbf{Q}\boldsymbol{\Lambda}^{-1}\mathbf{Q}^{\mathrm{T}} (\boldsymbol{v}_{\mathrm{T}} - \boldsymbol{f}(\boldsymbol{\theta})) = \sum_{i=1}^{(m+1)n} \frac{1}{\lambda_i} \left( (\boldsymbol{v}_{\mathrm{T}} - \boldsymbol{f}(\boldsymbol{\theta}))^{\mathrm{T}} \boldsymbol{e}_i \right)^2 \tag{30}$$

## 4 Simulations

### 4.1 Simulation Based on Human Kappa Opioid Occupancy Study

Simulations were performed based on real data from an occupancy study in humans (Naganawa et al. 2016) using the radiotracer $^{11}$C-LY2795050 targeting kappa opioid receptors (See Sect. 5.1.1 for details). The brain regions included in this simulation were the cerebellum, the amygdala, the caudate nucleus, the putamen, the pallidum, the thalamus, the insula, the hippocampus, and the anterior cingulum, posterior cingulum, frontal, occipital, and temporal cortices.

To generate ground truth parameters, real data from one subject were fitted using MA1 to obtain $V_{\mathrm{T}}$ values for a baseline scan and two post-drug scans. These $V_{\mathrm{T}}$ values were then used to estimate this subject's $V_{\mathrm{ND}}$ with Eq. (20) (Cunningham et al. 2010). To simulate data, we used the 4-parameter 2TC model; $V_{\mathrm{T}}$ and $V_{\mathrm{ND}}$ provide values for 2 of the 4 parameters. To provide the 2 additional parameter values, this subject's baseline time-activity curves were fitted with the 2TC model with the following constraints: $K_1 / k_2$ was fixed to the previously estimated $V_{\mathrm{ND}}$ in all ROIs, and $V_{\mathrm{T}}$ was fixed to the previously estimated MA1 $V_{\mathrm{T}}$ values. This produced a set of reference baseline parameters ($K_1$, $k_2$, $k_3$, $k_4$). To simulate post-drug data at a range of occupancy values $r$, $k_3$ was multiplied by $(1 - r)$. Simulated $r$ values ranged from 0.1 to 0.9 (with a step of 0.1). For convenience, the 2TC model was reparameterized, using the parameters $K_1$, $k_2$, $V_{\mathrm{T}}$, $k_4$ instead of $K_1$, $k_2$, $k_3$, $k_4$.

To simulate noisy occupancy studies, noise was added directly to the $V_{\mathrm{T}}$ values used to estimate the occupancy. Using the reference kinetic parameters previously determined, their covariance matrix was also estimated using Eq. (12) with weights as in Eq. (11), and assuming that the noise in the PET TACs could be modeled by Eq. (9). Since fits of simulated noisy TACs were not actually performed, the scale factor $\alpha$ was used to determine $s^2$.

To estimate the scale factor $\alpha$ in the noise formula, 2TC fits were performed for all scans in the real occupancy study using weights, as in (11), and $\alpha$ was estimated using Eq. (10). Then for each ROI $i$, the median value of $\alpha$ was computed to express a typical level of noise for this tracer. Simulations were also performed with all $\alpha_i$ increased by a factor of 9, i.e., threefold higher standard deviation.

For simulations with noise due to the input function according to the model shown in Eq. (16), $\sigma_{\mathrm{aif}}$ was set to 1, 3, 5, or 10%. As an example, based on 15 pairs of test/retest PET scans (Naganawa et al. 2015) which can provide an estimate of these effects, $\sigma_{\mathrm{aif}}$ was estimated to be $\sim$3% using Eq. (19). However, other tracers have poorer test/retest variability, often due to measurement errors in the input function. We simulated errors up to 10% since other tracers have poorer test/retest variability, in part due to larger measurement errors in the input function.

For each simulation case, 10,000 sets of 130 regional $V_T$ values (13 at baseline, 13 at each of the 9 occupancy levels) were generated. For each set of simulated $V_T$ values, occupancy estimates, $r$, were obtained using the OCCPLOT, ML-OLS, ML-WLS, and ML-FCM methods. These methods also provide estimated standard errors on the occupancy estimate ($SE_r$). To evaluate the accuracy of $SE_r$, the bias on $SE_r$ was computed with respect to the sample standard deviation across 10,000 replicates as $\text{median}(SE_r)/\text{sd}(r) - 1$.

Simulations were also performed for the case of multiple post-drug scans, in order to evaluate the usefulness of coupled fits to reduce variability, particularly for low occupancy studies. Simulations were performed for a pair of high (0.8) and low (0.2) occupancy scans, and for two levels of input function noise: no noise or 10% noise.

### 4.2 Simulation Results

Results of the method comparisons with simulations are shown in the form of Bland–Altman plots. For the simulation, results are plotted versus the ground truth in Figs. 2 and 3. There is one subplot for each method, i.e., the occupancy plot (OCCPLOT), ordinary least squares (ML-OLS), weighted least squares (ML_WLS), and the full covariance matrix maximum likelihood method (ML-FCM). A superior method would have a mean error near 0, and a small standard deviation.

The results of simulations with noise from the PET data only, i.e., without noise due to the input function ($\sigma_{aif} = 0$), are shown in Fig. 2. Occupancy estimates were more variable with the OCCPLOT and ML-OLS methods than with the ML-WLS method. Moreover, at the higher noise level, OCCPLOT estimates were more biased than the other methods. Since no noise contribution from the input function was added, the covariance matrix of the $V_T$ estimates is diagonal, and thus the ML-WLS and ML-FCM methods are identical. With the OCCPLOT method, the variability of occupancy estimates increased when the simulated occupancy was lower. With the other methods, variability of occupancy estimates was highest when the simulated occupancy was $\sim$30%, and the variability was lower for either high or low simulated occupancies.

The nondisplaceable volume of distribution $V_{ND}$ was also estimated. For all methods, the standard deviation of $V_{ND}$ estimates was higher at lower occupancy levels than at high occupancy levels. The relative standard deviations of $V_{ND}$ estimates were 5, 6, 2 and 2% for the OCCPLOT, ML-OLS, ML-WLS and ML-FCM methods, respectively, at high occupancy (70–90%), and $>$ 100, 47, 24, and 24%, respectively, at low occupancy (10–30%). Thus, the OCCPLOT method was by far the least stable method to estimate $V_{ND}$.

Using the OCCPLOT method, the standard errors of the occupancy estimates $SE_r$ were underestimated. The underestimation was higher for low occupancy simulations: the bias ranged from $-40$% for a 90% occupancy case, to $-54$% for a 10% occupancy case. This incorrect estimation of $SE_r$ was similar on average for ML-OLS, but with a different sensitivity to the level of occupancy: the bias was about $-41$% at 90% occupancy, peaked at $-53$% at 40% occupancy and $-23$% at 10% occupancy. The estimation of $SE_r$ was more accurate for ML-WLS (and ML-FCM), with a mean bias of only $-4$% across all occupancy levels; accurate standard error estimates are expected in this case, since all assumptions were met.

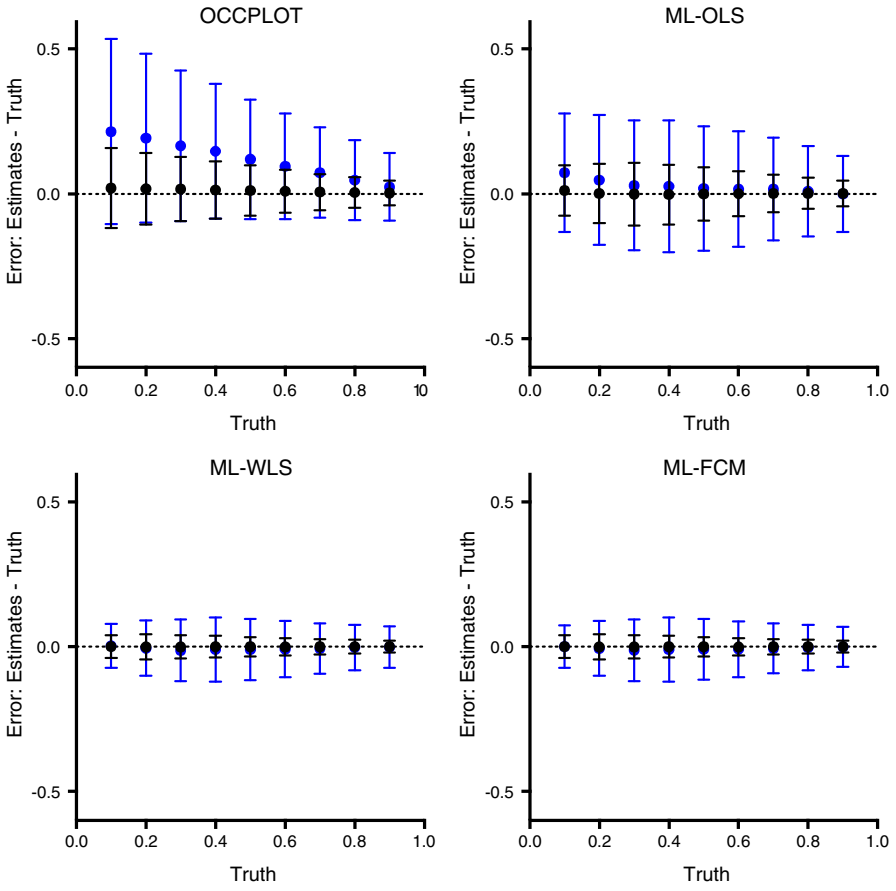


**Fig. 2** Bland–Altman plots of the error between occupancy estimates and simulated occupancies as a function of the simulated occupancy, when the input function is assumed to be noise free. Symbols show the mean error, and error bars show the standard deviation of the error. Data in black are from simulations at a typical PET noise level. Data in blue are from simulations with PET noise at a level 3 times higher (Color figure online)

A sample covariance matrix of the $V_T$ values used in simulations with noise due to the input function ($\sigma_{aif} = 5\%$) is shown in Table 1. The results of the simulations with $\sigma_{aif}$ set to 10% are shown in Fig. 3. The presence of (additional) noise in the input function increased the standard deviation in all methods, especially for ML-WLS, which provided slightly less variable results than ML-OLS in these simulations. As expected, ML-FCM provided less variable results than ML-WLS. The standard deviation of $r$ for simulated occupancy of 50% and various levels of input function noise are listed in Table 2. As expected, the difference in variability between ML-WLS and ML-OLS was reduced as input function noise increased. Conversely, the advantage of ML-FCM over ML-WLS became more apparent as input function noise increased.

Finally, the standard errors of the occupancy estimates $SE_r$ were underestimated for OCCPLOT, ML-OLS and ML-WLS, with average bias of $-58$, $-63$, and $-55\%$,

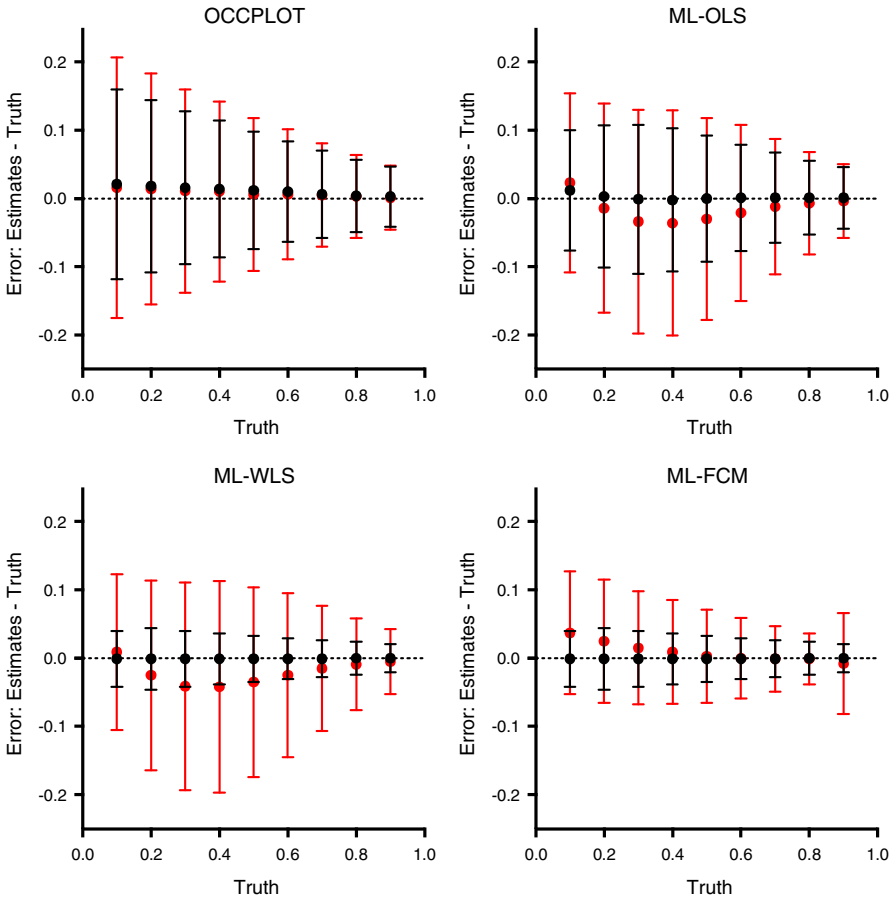


**Fig. 3** Bland–Altman plots of the error between occupancy estimates and simulated occupancies as a function of the simulated occupancy, with simulated noise from the input function ($\sigma_{aif}$=10%; red) or without simulated noise from the input function (black; repeated from Fig. 2 to allow direct comparison). Symbols show the mean error, and error bars show the standard deviation of the error (Color figure online)

respectively, when $\sigma_{aif}$ was set to 10% (average bias computed across all simulated occupancy values). ML-FCM provided relatively unbiased $SE_r$ values at higher occupancy levels (mean bias was 2% at occupancies $\geq$ 50%) but underestimated the standard deviation of occupancy values for low simulated occupancies (the bias was +39% at 10% occupancy).

Limited simulations were performed to assess the proposed methodology for multiple post-drug scans. Specifically, the ability of coupled fits to reduce the variability of low occupancy studies by analyzing data jointly with a high occupancy study in the same subject was tested using a pair of studies with simulated occupancies of 0.8 and 0.2. When no noise was added to the input function data, all coupled methods (ML-OLS2, ML-WLS2, ML-FCM2) showed lower variability for the low occupancy study. Comparing single- to paired-scan analysis, the standard deviation of errors was reduced from 0.10 to 0.058 for ML-OLS2, and from 0.044 to 0.019 for ML-WLS2 and

**Table 1** $V_T$ covariance matrix[a] for 5% input function noise level

| Diagonal block | ROI | Cer | Amy | Cau | ACin | PCin | Fro | Hip | Pal | Ins | Occ | Put | Tem | Tha |
|---|---|---|---|---|---|---|---|---|---|---|---|---|---|---|
| Baseline | Cer | **7.1** | 12.9 | 6.2 | 10.2 | 6.6 | 8.1 | 7.2 | 10.0 | 10.5 | 8.0 | 9.8 | 8.7 | 7.0 |
| Baseline | Amy | 12.9 | **121.9** | 12.6 | 20.7 | 13.3 | 16.4 | 14.6 | 20.3 | 21.3 | 16.2 | 19.9 | 17.6 | 14.1 |
| Baseline | Cau | 6.2 | 12.6 | **8.5** | 10.0 | 6.4 | 7.9 | 7.1 | 9.8 | 10.3 | 7.8 | 9.6 | 8.5 | 6.8 |
| Baseline | ACin | 10.2 | 20.7 | 10.0 | **20.5** | 10.5 | 12.9 | 11.6 | 16.1 | 16.8 | 12.8 | 15.7 | 13.9 | 11.2 |
| Baseline | PCin | 6.6 | 13.3 | 6.4 | 10.5 | **40.7** | 8.3 | 7.4 | 10.3 | 10.8 | 8.2 | 10.1 | 8.9 | 7.2 |
| Baseline | Fro | 8.1 | 16.4 | 7.9 | 12.9 | 8.3 | **11.6** | 9.2 | 12.7 | 13.3 | 10.1 | 12.5 | 11.0 | 8.8 |
| Baseline | Hip | 7.2 | 14.6 | 7.1 | 11.6 | 7.4 | 9.2 | **16.2** | 11.4 | 11.9 | 9.1 | 11.2 | 9.9 | 7.9 |
| Baseline | Pal | 10.0 | 20.3 | 9.8 | 16.1 | 10.3 | 12.7 | 11.4 | **21.5** | 16.5 | 12.6 | 15.5 | 13.7 | 11.0 |
| Baseline | Ins | 10.5 | 21.3 | 10.3 | 16.8 | 10.8 | 13.3 | 11.9 | 16.5 | **24.3** | 13.2 | 16.2 | 14.3 | 11.5 |
| Baseline | Occ | 8.0 | 16.2 | 7.8 | 12.8 | 8.2 | 10.1 | 9.1 | 12.6 | 13.2 | **11.3** | 12.3 | 10.9 | 8.7 |
| Baseline | Put | 9.8 | 19.9 | 9.6 | 15.7 | 10.1 | 12.5 | 11.2 | 15.5 | 16.2 | 12.3 | **16.3** | 13.4 | 10.7 |
| Baseline | Tem | 8.7 | 17.6 | 8.5 | 13.9 | 8.9 | 11.0 | 9.9 | 13.7 | 14.3 | 10.9 | 13.4 | **13.4** | 9.5 |
| Baseline | Tha | 7.0 | 14.1 | 6.8 | 11.2 | 7.2 | 8.8 | 7.9 | 11.0 | 11.5 | 8.7 | 10.7 | 9.5 | **9.4** |
| Blocked* | Cer | **4.4** | 4.5 | 3.9 | 4.3 | 4.0 | 4.1 | 4.0 | 4.2 | 4.3 | 4.1 | 4.2 | 4.1 | 4.0 |
| Blocked* | Amy | 4.5 | **14.1** | 4.5 | 4.8 | 4.5 | 4.6 | 4.5 | 4.8 | 4.8 | 4.6 | 4.8 | 4.7 | 4.5 |
| Blocked* | Cau | 3.9 | 4.5 | **5.3** | 4.2 | 4.0 | 4.1 | 4.0 | 4.2 | 4.3 | 4.1 | 4.2 | 4.1 | 4.0 |
| Blocked* | ACin | 4.3 | 4.8 | 4.2 | **5.3** | 4.3 | 4.4 | 4.3 | 4.6 | 4.6 | 4.4 | 4.5 | 4.5 | 4.3 |

**Table 1** continued

| Diagonal block | ROI | Cer | Amy | Cau | ACin | PCin | Fro | Hip | Pal | Ins | Occ | Put | Tem | Tha |
|---|---|---|---|---|---|---|---|---|---|---|---|---|---|---|
| Blocked* | PCin | 4.0 | 4.5 | 4.0 | 4.3 | **23.0** | 4.1 | 4.0 | 4.3 | 4.3 | 4.1 | 4.2 | 4.2 | 4.0 |
| Blocked* | Fro | 4.1 | 4.6 | 4.1 | 4.4 | 4.1 | **4.7** | 4.2 | 4.4 | 4.4 | 4.2 | 4.4 | 4.3 | 4.1 |
| Blocked* | Hip | 4.0 | 4.5 | 4.0 | 4.3 | 4.0 | 4.2 | **7.4** | 4.3 | 4.4 | 4.2 | 4.3 | 4.2 | 4.1 |
| Blocked* | Pal | 4.2 | 4.8 | 4.2 | 4.6 | 4.3 | 4.4 | 4.3 | **5.6** | 4.6 | 4.4 | 4.5 | 4.4 | 4.3 |
| Blocked* | Ins | 4.3 | 4.8 | 4.3 | 4.6 | 4.3 | 4.4 | 4.4 | 4.6 | **5.9** | 4.4 | 4.6 | 4.5 | 4.3 |
| Blocked* | Occ | 4.1 | 4.6 | 4.1 | 4.4 | 4.1 | 4.2 | 4.2 | 4.4 | 4.4 | **4.7** | 4.4 | 4.3 | 4.1 |
| Blocked* | Put | 4.2 | 4.8 | 4.2 | 4.5 | 4.2 | 4.4 | 4.3 | 4.5 | 4.6 | 4.4 | **4.8** | 4.4 | 4.3 |
| Blocked* | Tem | 4.1 | 4.7 | 4.1 | 4.5 | 4.2 | 4.3 | 4.2 | 4.4 | 4.5 | 4.3 | 4.4 | **4.7** | 4.2 |
| Blocked* | Tha | 4.0 | 4.5 | 4.0 | 4.3 | 4.0 | 4.1 | 4.1 | 4.3 | 4.3 | 4.1 | 4.3 | 4.2 | **4.8** |

Bolded items identify the diagonal values of the matrix

*Simulated occupancy was 90%

[a]Values are scaled up by a factor of 1,000, for display purposes

**Table 2** Standard deviation of occupancy estimates* for various input function noise levels

| Noise level (%) | OCCPLOT | ML-OLS | ML-WLS | ML-FCM |
|---|---|---|---|---|
| 0 | 0.086 | 0.092 | 0.034 | 0.034 |
| 1 | 0.087 | 0.092 | 0.035 | 0.034 |
| 3[a] | 0.089 | 0.095 | 0.044 | 0.040 |
| 5 | 0.094 | 0.101 | 0.062 | 0.049 |
| 10 | 0.112 | 0.148 | 0.139 | 0.068 |

*OCCPLOT* occupancy plot, *ML* maximum likelihood, *OLS* ordinary least squares, *WLS* weighted least squares, *FCM* full covariance matrix

*Simulated occupancy was 50%; $n = 10{,}000$ replicates

[a]Input function noise level estimated on real data based on test/retest studies

ML-FCM2, i.e., ∼50% variability reduction for all methods. There were negligible effects on the variability of the high occupancy estimates. However, with $\sigma_{\text{aif}}$ set to 10% noise, coupled fitting increased variability for methods that did not use the full covariance matrix: the standard deviation of errors increased from 0.15 to 0.18 for ML-OLS2, and from 0.14 to 0.19 for ML-WLS2. Conversely, the standard deviation of errors decreased with ML-FCM2 as expected, from 0.090 to 0.073, though this reduction was smaller (∼20%) than that in the simulation without AIF noise.

## 5 Real Data

### 5.1 Kappa Occupancy Study

Results of the method comparisons with real data are shown in the form of Bland–Altman plots. Since no gold standard is available for the real data, results (Figs. 4, 5, 6, 7) are plotted vs. those estimated using ML-FCM, since ML-FCM produced the minimum bias in the simulation. These plots should be interpreted in light of the results from the simulation (Figs. 2, 3), to see if the same between-method pattern is visible.

#### *5.1.1 Occupancy Study Methods*

Data obtained from 7 healthy subjects scanned with the kappa opioid receptor tracer $^{11}$C-LY2795050 were used to test the occupancy estimation methods. The occupancy studies were conducted with the drug LY2456302 as described in (Naganawa et al. 2016). Briefly, each subject underwent three PET scans (a baseline and two post-drug scans at 2 and 24 h post-drug), each for 90 min on the High Resolution Research Tomograph (HRRT) scanner. Metabolite-corrected arterial input functions were measured. A range of LY2456302 doses was evaluated in this study: 0.5 mg ($n = 1$), 2 mg ($n = 3$), 4 mg ($n = 2$), 10 mg ($n = 1$). Time-activity curves (TACs) of the following 13 ROIs were analyzed: amygdala, caudate, anterior cingulate cortex, posterior cingulate cortex, frontal cortex, hippocampus, insula, occipital cortex, pallidum, putamen, temporal cortex, thalamus, and cerebellum. $V_{\text{T}}$ values were estimated for each ROI and scan using MA1 (Ichise et al. 2002) with $t^* = 20$ min.

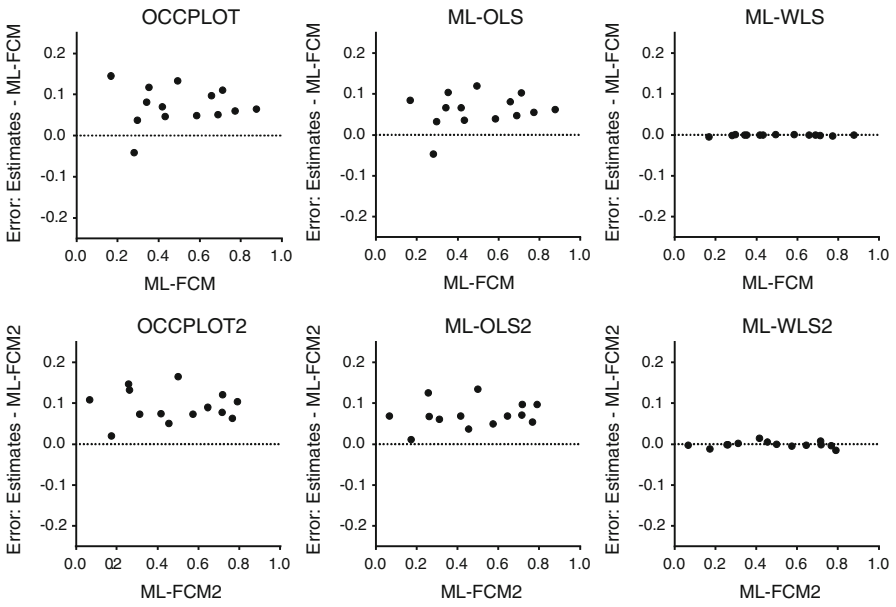


**Fig. 4** Bland–Altman plots of the difference between occupancy estimates from $^{11}$C-LY2795050 PET data using different methods and the ML-FCM estimates [ML-FCM (top) and ML-FCM2 (bottom)]. The *x* axis values were taken from ML-FCM or ML-FCM2 estimates, respectively. Each data point denotes an occupancy value from a pair of baseline and post-dose scans

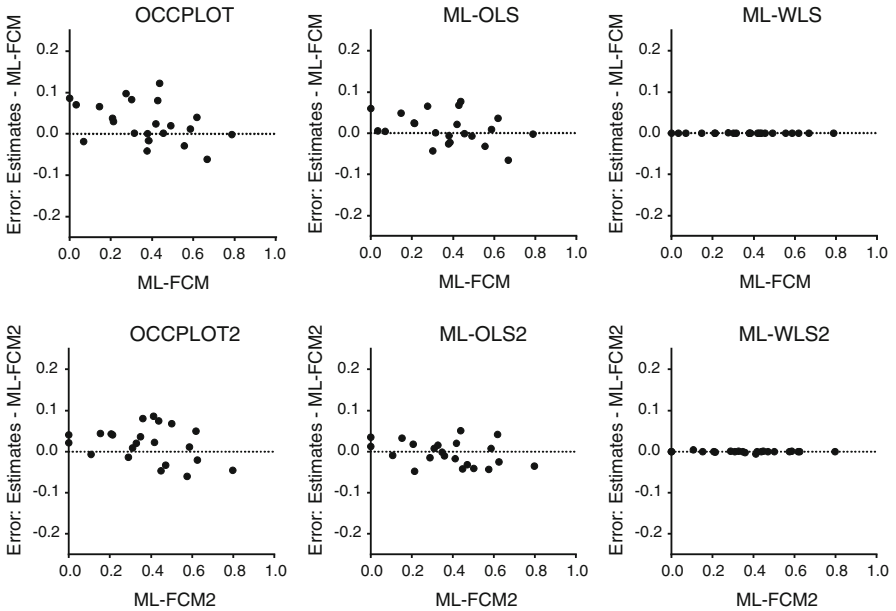


**Fig. 5** Bland–Altman plots of the difference between occupancy estimates from $^{18}$F-MK-6577 PET data using different methods and ML-FCM estimates [ML-FCM (top) and ML-FCM2 (bottom)]. The *x* axis values were taken from ML-FCM or ML-FCM2 estimates, respectively. Each data point denotes an occupancy value from a pair of baseline and post-dose scans

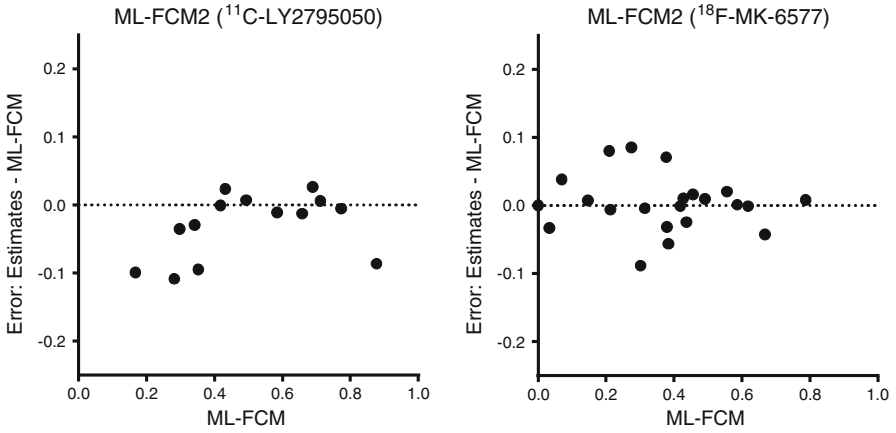


**Fig. 6** Bland–Altman plots of the difference between occupancy estimates from $^{11}$C-LY2795050 (left) and $^{18}$F-MK-6577 (right) PET data using ML-FCM2 and ML-FCM estimates. Each data point denotes an occupancy value from a pair of baseline and post-dose scans

### *5.1.2 Occupancy Calculations*

$V_T$ values were computed with OCCPLOT, ML-OLS, ML-WLS, and ML-FCM. Since all subjects had two post-drug scans, the data were also analyzed with OCCPLOT2, ML-OLS2, ML-WLS2, and ML-FCM2. For ML-WLS, relative variances of regional distribution volumes were chosen based on the PET ROI noise model and theoretical covariance matrix as described in Sect. 4.1, but noise from the input function was not considered. For ML-FCM, $\sigma_{\text{aif}}$ was set to 3%, and the same regional scale factors, $\alpha$, were used as in the simulation.

### *5.1.3 Occupancy Results*

Occupancy estimates using the OCCPLOT, ML-OLS, and ML-WLS methods were compared with those estimated using ML-FCM (Fig. 4, top). In the absence of a gold standard, since ML-FCM produced the minimum bias in the simulation, the ML-FCM estimate was taken as the true value for the $x$ axis of the Bland–Altman plots. Compared with the ML-FCM estimates, the OCCPLOT and ML-OLS methods showed larger estimated results, while the ML-WLS estimates were very similar to the ML-FCM estimates. The mean and standard deviation of the difference between the estimated occupancies (bias) and ML-FCM estimates were $7.3 \pm 4.7$, $6.1 \pm 4.1$, and $-0.1 \pm 0.1\%$ for the OCCPLOT, ML-OLS, and ML-WLS methods, respectively. No trend was found between the bias and the occupancy estimated using the ML-FCM method ($P > 0.5$).

Occupancy estimates using the OCCPLOT2, ML-OLS2, and ML-WLS2 were compared with those estimates using ML-FCM2, and similar results were found (Fig. 4, bottom). The mean and standard deviation of the difference with respect to ML-FCM2 estimates were $9.3 \pm 3.9$, $7.2 \pm 3.3$, and $-0.1 \pm 0.7\%$ for the OCCPLOT2, ML-OLS2, and ML-WLS2 methods, respectively.

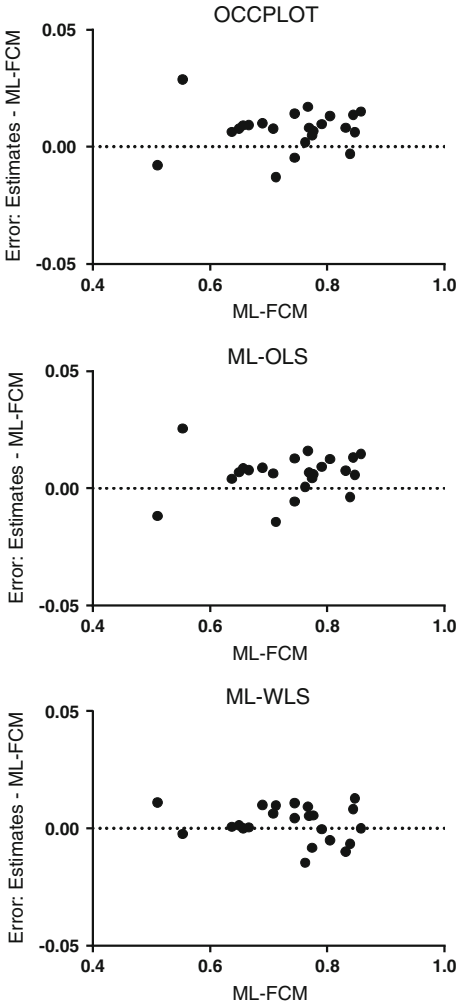


**Fig. 7** Bland–Altman plots of the absolute error between occupancy estimates from $^{11}$C–UCB–J PET data using OCCPLOT (top), ML-OLS (middle), ML-WLS (bottom), and ML-FCM methods. The *x* axis values were taken from ML-FCM. Each data point denotes an occupancy value from a pair of baseline and post-dose scans

Comparing ML-FCM and ML-FCM2 occupancy estimates (Fig. 6, left), ML-FCM2 occupancy tended to be lower than ML-FCM occupancy. The largest differences were seen in the scans with occupancy $< 40\%$.

## 5.2 Glycine Transporter Occupancy Study

### *5.2.1 Occupancy Study Methods*

Data obtained from 6 healthy subjects and 5 schizophrenia patients scanned with the glycine transporter 1 (GlyT1) tracer $^{18}$F-MK-6577 (Joshi et al. 2015) were used to test the occupancy estimation methods. The occupancy studies were conducted with the GlyT1 inhibitor (PF-03463257). All subjects were assigned to three treatment

groups based on a combination of placebo (baseline) and two out of three doses of PF-03463257 (10, 20, and 40 mg). In each treatment period, subjects received the medication twice daily for 7 days. Each subject underwent three PET scans on the HRRT scanner for 90 min at baseline and at steady state of each dose received: Metabolite-corrected arterial input functions were measured. Regional TACs of 20 ROIs, including cortical regions, striatum, midbrain, pons, and cerebellum, were analyzed. $V_T$ values were estimated for each ROI and scan using MA1 (Ichise et al. 2002) with $t^* = 40$ min.

#### *5.2.2 Occupancy Calculations*

The GlyT1 data were analyzed with the same procedure as described in Sect. 5.1.2. For ML-FCM, $\epsilon_{aif}$ was set to 3%, and the ROI noise scale factors, $\alpha$, were computed from the GlyT1 data using the method described in Sect. 4.1.

#### *5.2.3 Occupancy Results*

Occupancy estimates using the OCCPLOT, ML-OLS, and ML-WLS methods were compared with those estimated using ML-FCM. The estimated results are shown in Fig. 5 (top). Occupancy estimates with the ML-OLS method were less variable than the estimates with the OCCPLOT method. The ML-WLS occupancy estimates were almost identical to the ML-FCM occupancy estimates. The mean and standard deviation of the difference between estimated occupancies (bias) and ML-FCM estimates were $2.7 \pm 4.9$, $1.1 \pm 3.8$, and $0.0 \pm 0.0\%$ for the OCCPLOT, ML-OLS, and ML-WLS methods, respectively. The bias appeared to be reduced at higher occupancy levels.

Occupancy estimates using the OCCPLOT2, ML-OLS2, and ML-WLS2 were compared with those estimates using ML-FCM2. Similar property was seen in the comparison (Fig. 5, bottom). The mean and standard deviation of the difference between bias and ML-FCM2 estimates were $1.9 \pm 4.3$, $-0.4 \pm 3.0$, and $0.0 \pm 0.2\%$ for the OCCPLOT2, ML-OLS2, and ML-WLS2 methods, respectively.

Comparing ML-FCM and ML-FCM2 occupancy estimates (Fig. 6, right), ML-FCM2 occupancy was similar to ML-FCM occupancy in the scans with occupancy $> 40\%$. For lower occupancy scans, the differences between ML-FCM and ML-FCM2 occupancies were more variable.

### 5.3 SV2A Occupancy Study

#### *5.3.1 Occupancy Study Methods*

The PET radiotracer $^{11}$C-UCB-J targets synaptic vesicular protein (SV2A) and can be used as a marker for synaptic density in humans (Finnema et al. 2016). This protein is the site of action of the antiepileptic drugs Brivaracetam (BRV) and Levetiracetam (LEV), and PET scans with $^{11}$C–UCB–J can be used to assess drug occupancy. Using $^{11}$C-UCB-J PET with a bolus plus infusion protocol, a total of 23 pairs of baseline and blocking scans were completed across 9 healthy controls who received varying doses of BRV and/or LEV. Regional TACs of 23 ROIs including gray matter regions

of the cerebral cortex, subcortical regions, striatum, midbrain, and cerebellum were used for analysis. Using 60-min of data from baseline and blocking data, regional $V_T$ values were estimated with the 1TC model, and occupancy was estimated for each pair of scans. In some cases, the baseline scan was performed on the same day as the blocking scan. In other cases, the blocking scan was performed on a subsequent day following chronic dosing.

#### *5.3.2 Occupancy Calculations*

SV2A occupancy data were analyzed with methods similar to those described in 5.1.2 and 5.2.2, in which regional $V_T$ values were used with OCCPLOT, ML-OLS, ML-WLS, and ML-FCM. For ML-FCM, the $\varepsilon_{aif}$ was set to 3%, and the regional noise level $\alpha$ was determined from the data, as described in section 4.1.

#### *5.3.3 Occupancy Results*

SV2A occupancy estimates from OCCPLOT, ML-OLS, and ML-WLS methods were compared to those from the ML-FCM method, under the assumption that ML-FCM provides true occupancy values, based on the simulation results. All occupancies were high ($> 50\%$), and each method provided occupancy estimates of comparable variability.

Occupancy estimates derived from OCCPLOT, ML-OLS, and ML-WLS were compared to those derived from ML-FCM (Fig. 7). Differences between methods were extremely small. The mean and standard deviation of the percent difference between the estimated occupancies and the ML-FCM occupancy estimates were $1.0 \pm 1.4$, $0.8 \pm 1.4$, and $0.3 \pm 1.0\%$ for OCCPLOT, ML-OLS, and ML-WLS, respectively.

## 6 Discussion Topics

### 6.1 Overview of This Work

The goal of this work is to provide more accurate and precise estimates of target occupancy from PET studies. This work was motivated in part by the routine use of the convenient occupancy plot (Cunningham et al. 2010). This plot is used commonly because of its appealing nature, where data are plotted and the relevant parameter, $r$, is the slope of the plot. This style of analysis, i.e., plotting the data in a way to make the slope of a line the relevant parameter has a long history in PET, as evidenced by the Patlak and Logan plots (Logan et al. 1990b; Patlak et al. 1983) for irreversible and reversible tracers, respectively. However, the occupancy plot suffers from incorrect statistical assumptions, so the purpose of our work was to improve the statistical characteristics of the estimates of $r$ (and $V_{ND}$). Also, fitting the slope of the occupancy plot ignores regional differences in the variability of the $V_T$ values. Such between-region noise differences can be caused by variation in region size or noise differences in $V_T$ estimation. For example, high $V_T$ values can often have high %SE for studies with the short half-life of $^{11}C$, since the region approaches equilibrium slowly.

An additional goal is to produce a reliable estimate of the standard error of these estimates, a value which cannot be reliably obtained from the occupancy plot. Such a standard error would be helpful when using $r$ values from multiple experiments to estimate a drug $IC_{50}$, e.g., as we performed recently using the kappa opioid ligand $^{11}$C–LY2795050 (Naganawa et al. 2016). An accurate standard error of $r$ would be particularly helpful if there is substantial variability in the reliability of the individual $r$ values, e.g., due to substantial differences in injected tracer dose per subject.

In this work, we chose to limit the analysis to cases where there is no reference region, i.e., a region devoid of specific binding. In fact, demonstration that a region is in fact an ideal reference region requires that the $V_T$ of the reference region is equal to (or very close to) $V_{ND}$, i.e., $V_S$ is nearly 0. Thus, validation of a reference region requires an accurate and reliable estimate of $V_{ND}$, which is obtained from these occupancy studies.

### 6.2 Sources of Error Common to Multiple Regions/Organs from One Scan

Many investigators have analyzed PET kinetic data and included weighting of the individual data points to account for noise differences, typically due to activity level and radioactive decay (Yaqub et al. 2006). There are many such models which, in general, tend to produce minor difference in PET fitted values, except in cases where there are large differences in noise level between-scan frames. However, when multiple modeling results are obtained from a single dynamic scan, there are many other noise sources that produce common or similar noise in all the regional values, so the regional estimates are correlated. Some sources of these correlations come from the physiological modeling and include 1) the use of a common time-activity curve in plasma, 2) the use of a common plasma metabolite correction, and 3) the effect of plasma-free fraction ($f_P$), either due to ignoring this effect or due to noise in its correction. Other factors are based on the scanner physics such as the calibration factors, as well as image processing steps, including registration of PET to MR or CT scans and subsequent registration to atlases for region definition. Some of these issues can cause correlation of values between baseline and post-drug scans, such as the use of a common MR image to process both datasets. Thus, accurate definition of the covariance matrix of the vector of $V_T$ values from one or multiple scans is challenging and has not been addressed in the PET literature.

Here, we used approximations for this covariance matrix to assess the impact of including these off-diagonal terms on the estimates of $r$. However, in future studies, it may be possible to provide a better estimate of the covariance matrix. One approach, which we applied here, is to use test/retest data (Naganawa et al. 2014, 2015; Normandin et al. 2015; Park et al. 2015; Saricicek et al. 2015) to understand the within-scan and between-scan correlations. Use of test/retest data avoids the confound of separating within-subject and between-subject variance. Proper estimation is likely to require a large dataset, so analysis of multiple studies with different tracers may be needed. Also, in general, test/retest studies of drug occupancy are rarely done, so extrapolations from baseline to post-drug scans will be needed. Such extrapolations should account for the reduced $V_T$ values that occur in post-drug scans. Specifically,

estimation of $V_T$ is most often improved in post-drug scans, since the tissue TACs approach equilibrium more quickly, thus reducing the SE of $V_T$.

### 6.3 Simulation Results

All four methods provided similarly unbiased occupancy estimates at typical ROI noise levels in the simulations based on the $^{11}$C–LY2795050 tracer (Fig. 2). The OCCPLOT method was slightly (positively) biased at higher noise levels. Some bias is expected for a graphical analysis such as the OCCPLOT method, due to the presence of noise in the independent variables, and additionally due to the correlation between this noise and the noise in the dependent variables. However, the bias in the OCCPLOT method is not as large as in some other graphical analysis, e.g., the graphical analysis used to estimate $V_T$ values for reference tracers (Slifstein and Laruelle 2000). The direction of the bias (overestimation), and the observation that the bias is relatively larger for low-dose studies is consistent with results shown previously (Cunningham et al. 2010).

The main difference between methods was seen in the variability of the occupancy estimates, which was lower in the ML-WLS method (in simulations without noise terms due to the input function), or the MLS-FCM method (in simulations with large input function noise terms, $\epsilon_{aif}$). Thus, ML-WLS and ML-FCM methods will be useful to improve occupancy estimates using tracers for which $V_T$ estimates have varying noise in different ROIs. Regional $V_T$ estimates will have different levels of noise due to the different ROI sizes, regional tracer uptake levels, and kinetic properties (e.g., low flow regions and high binding regions are expected to have more variable $V_T$ estimates due to the slower washout of the tracer from these regions). The ML-FCM method will be more useful for tracers in which the input function estimation process contributes a large fraction of the overall variability of $V_T$ estimates. In this simulation, the sample standard deviation of $r$ estimates did not differ between ML-WLS and ML-FCM until $\epsilon_{aif}$ was at least 5%. However, identifying these tracers and developing accurate model of the noise for real data is still an open question.

In addition, the standard errors on the occupancy estimates were underestimated by OCCPLOT and ML-OLS methods compared to the actual standard deviation of occupancy estimates. ML-WLS also underestimated the standard errors on the occupancy estimates for simulated studies with high noise levels from the input function.

### 6.4 Real-Data Results

In the simulation, occupancy estimates were more variable with OCCPLOT and ML-OLS and the variability tended to be larger for lower occupancy. These patterns were not evident in the real data, in part because of too few data points to quantify the variability as a function of occupancy level. For $^{18}$F–MK-6577 (Fig. 5), there was no clear pattern of bias between the various methods, although OCCPLOT may have had a positive bias for low occupancy values. The bias pattern was different for $^{11}$C–LY2795050 (Fig. 4), where a positive bias of 6–9% was seen for OCCPLOT and ML-OLS; this bias was uniform over occupancy values. This pattern suggests that

there is another source of bias due to a violation of one or more assumptions of the general occupancy model (see below).

For $^{11}$C–UCB–J (Fig. 7), results from all methods were effectively identical. For this tracer, the statistical precision of the $V_T$ values is excellent due to high tracer uptake (low data noise), and the use of a simple 1TC model to estimate $V_T$. Also, the dynamic range of $V_T$ values is small for this tracer, and in the studies used here, occupancy values were high. These factors contributed to very small differences between methods for this tracer.

In all real-data cases, ML-WLS and ML-FCM gave virtually identical results. This was the case because the presumed error in the input function was assumed to be small (3%). The value of 3% was chosen from test/retest data of a number of studies, but would be more appropriately determined individually for each tracer.

Figure 6 shows the effect of simultaneously analyzing data from 2 post-drug occupancy studies, and assuming a common nondisplaceable volume of distribution ($V_{ND}$) between all scans. Looking at the data from both tracers, there is some evidence of more variability in ML-FCM at low occupancy values. This is not surprising, since the precise estimation of both $r$ and $V_{ND}$ is generally challenging for low occupancy studies. By simultaneously fitting 2 $r$ values and 1 $V_{ND}$ value from one baseline and 2 post-drug scans in ML-FCM2, effectively, the higher-precision information of $V_{ND}$ provided by the high occupancy scan improves the $r$ estimation for the low occupancy scan. Also, the differences between single- and paired-scan analyses in the real data were consistent with the simulation, i.e., simultaneous analysis of multiple post-drug scans reduced variability in low occupancy scans, with negligible changes in high occupancy results.

## 6.5 Extensions for Other Scenarios

### *6.5.1 Reference Region Data Available*

If a suitable reference region is available, then the binding potential can be determined for multiple regions [Eq. (2)]. If blocking studies are then performed, the occupancy can be determined for region $i$ ($r_i$) with Eq. (5). There are then multiple simple methods to estimate the global occupancy, e.g., unweighted or weighted averages of the $r_i$. Weighted or unweighted averages of $BP_{ND}$ values across regions could be performed first, and then $r$ calculated using Eq. (5) with the baseline and post-drug average $BP_{ND}$ values. Alternatively, full maximum likelihood versions for estimation, as in Eq. (23), could be implemented, where $\boldsymbol{\theta} = \left[\frac{V_{S,1}}{V_{ND}}, \frac{V_{S,2}}{V_{ND}}, \ldots, \frac{V_{S,n}}{V_{ND}}, r\right]$ is the ($n$+1)-vector of parameters to estimate, $v_T$ is a vector of the measured $BP_{ND}$ values at baseline and post-drug administration ($2n$ values), and $\boldsymbol{f}(\boldsymbol{\theta})$ is the model function as shown in Eqs. (2) and (4). As in our work, such an implementation would ideally include an appropriate $\boldsymbol{\Sigma}$, the $2n$-by-$2n$ $BP_{ND}$ covariance matrix. To determine this matrix, would require consideration of all the issues described in Sect. 6.2, as well as including the effect of the use of common reference region data in the calculation of all $BP_{ND}$ values in a single scan, introducing another source of between-measure covariance.

### 6.5.2 Single-Subject $IC_{50}$ Estimation

Occupancy can be expressed in terms of free drug concentration as

$$r = \frac{C}{C + IC_{50}} \tag{31}$$

where $C$ is the free drug concentration at the target site and $IC_{50}$ is the half-maximal inhibitory concentration, i.e., the drug concentration in the plasma that is required to achieve 50% occupancy of the target site. The equations in this section also hold by replacing $C$ and $IC_{50}$ by $D$ and $ID_{50}$, respectively, where $D$ is the administered dose of the drug and $ID_{50}$ is the half-maximal inhibitory dose; this assumes that the post-drug scans are acquired at similar times post-dosing.

One of the main purposes of an occupancy study is to estimate $IC_{50}$ from a dose–response curve (occupancy vs. drug concentration). The $IC_{50}$ value can be estimated from data of a single subject. Consider a case of $m$ post-drug scans. The measured $V_T$ values of the $i$th ROI at baseline scan and $k$th post-drug scan are modeled as:

$$V_{T,\mathrm{base,i}} = V_{ND} + V_{S,i} + \varepsilon_i \tag{32}$$

$$V_{T,\mathrm{post},i,k} = V_{ND} + \left(1 - \frac{C_k}{C_k + IC_{50}}\right) V_{S,i} + \varepsilon_i \ (k = 1, \ldots, m) \tag{33}$$

where $\varepsilon_i$ is additive Gaussian noise and $C_k$ is the drug concentration at the target site during the $k$th post-drug scan.

Let $\boldsymbol{\theta} = \left[V_{S,1}, V_{S,2}, \ldots, V_{S,n}, V_{ND}, IC_{50}\right]$ be the vector of parameters to estimate. The elements of $\theta$ are estimated by minimizing a cost function

$$g(\boldsymbol{\theta}) = (\boldsymbol{v}_T - \boldsymbol{f}(\boldsymbol{\theta}))^T \boldsymbol{\Sigma}^{-1} (\boldsymbol{v}_T - \boldsymbol{f}(\boldsymbol{\theta})) \tag{34}$$

where $\boldsymbol{v}_T$ is a vector of the measured distribution volumes at baseline and post-drug administration ($n(m+1)$ values) and $\boldsymbol{\Sigma}$ is the $n(m+1)$ -by-$n(m+1)$ data covariance matrix. $\boldsymbol{f}(\boldsymbol{\theta})$ is the model function as shown in Eqs. (32) and (33). Proper definition of $\boldsymbol{\Sigma}$ should also include error sources due to uncertainty in $C_k$ values; alternatively, the $C_k$ values could be added to the data vector and the true concentrations could be added to the parameter vector $\boldsymbol{\theta}$.

## 6.6 Occupancy Estimates Without a Baseline Scan

When a subject has two post-drug scans with no baseline scan, Eq. (31) allows us to estimate occupancy for each using the following extensions of the occupancy plot (Cunningham et al. 2010):

$$\left(\boldsymbol{V}_{T,\mathrm{post},1} - \boldsymbol{V}_{T,\mathrm{post},2}\right) \frac{C_2}{C_2 - C_1} = r_{\mathrm{post},2} \left(\boldsymbol{V}_{T,\mathrm{post},1} - \boldsymbol{V}_{ND}\boldsymbol{u}\right) \tag{35}$$

$$\left(\boldsymbol{V}_{T,\mathrm{post},2} - \boldsymbol{V}_{T,\mathrm{post},1}\right) \frac{C_1}{C_1 - C_2} = r_{\mathrm{post},1} \left(\boldsymbol{V}_{T,\mathrm{post},2} - \boldsymbol{V}_{ND}\boldsymbol{u}\right) \tag{36}$$

where $C_1$ and $C_2$ are the measured drug concentrations for post-drug scans 1 and 2. Plotting $\left(\boldsymbol{V}_{\mathrm{T,post},1} - \boldsymbol{V}_{\mathrm{T,post},2}\right)\frac{C_2}{C_2 - C_1}$ ($y$-axis) versus $\boldsymbol{V}_{\mathrm{T,post},1}$ ($x$-axis) across $n$ regions leads to a linear relationship with a slope equal to $r_{\mathrm{post},2}$ and $x$ intercept equal to $V_{\mathrm{ND}}$. For this approach to be reliable, the difference in the drug concentrations between the post-drug scans should not be small.

Alternatively, we can use the maximum likelihood framework developed in section 6.5.2 to analyze these data. Using the same $\boldsymbol{\theta}$ vector ($n$+2 elements), $\boldsymbol{v}_{\mathrm{T}}$ is the data vector of the measured distribution volumes in all post-drug scans (nm values) and $\boldsymbol{\Sigma}$ is the nm -by-nm data covariance matrix.

### 6.7 Multi-Subject Analysis

Consider a case with more than one subject ($l > 1$) who underwent a baseline and $m$ post-drug scans. Assuming that the measured $V_{\mathrm{T}}$ values can be modeled using Eqs. (31) and (32), a cost function to be minimized is simply extended from Eq. (33) where $\boldsymbol{v}_{\mathrm{T}}$ is a vector of the measured distribution volumes at post-drug administration ($nl(m+1)$ values) and $\boldsymbol{\Sigma}$ is the $nl(m+1)$ -by-$nl(m+1)$ data covariance matrix. This approach can be implemented most simply by assuming no intersubject variation in $V_S$ values, $V_{\mathrm{ND}}$, or $IC_{50}$, i.e., the parameter vector is $\boldsymbol{\theta} = \left[V_{\mathrm{S},1,}, V_{\mathrm{S},2}, \ldots, V_{\mathrm{S},n}, V_{\mathrm{ND}}, IC_{50}\right]$.

A more sophisticated approach would incorporate population variability in all of these values, as well as an appropriate covariance matrix. A proper model for covariance in this case requires substantial understanding of both PET methodology, as described here, as well as the underlying biological variability, specific to the target biological system. For example, it would require adding subject-specific "noise" terms to the data model [Eq. (16)], and either providing these variances as known or estimating these terms from the data. However, in general, PET occupancy studies are small (e.g., 10–20 post-dose scans), so estimating these interindividual factors from the data is very challenging.

### 6.8 Assumptions of PET Occupancy Methods

For all PET occupancy studies including the studies presented here, the model of Eqs. (21) and (22), assume that nondisplaceable binding ($V_{\mathrm{ND}}$) is uniform across regions and that the target occupancy $r$ is also uniform. In order to assess the uniformity of $V_{\mathrm{ND}}$, a blocking study with a very high occupancy ($r \approx 1$) would be required, so that the measured $V_{\mathrm{T}}$ data are effectively equal to $V_{\mathrm{ND}}$. Often in human studies, this cannot be accomplished, due to limitations of drug dose caused by pharmacological effects. Thus, this assumption is more often tested in animal studies. For example, we recently assessed the validity of the uniform $V_{\mathrm{ND}}$ assumption for the glycine transporter tracer $^{18}$F-MK-6577 (Joshi et al. 2015) in a study in nonhuman primates (Xia et al. 2015). Using unlabeled MK-6577 as the drug at multiple doses, we estimated $V_{\mathrm{ND}}$ for every voxel of the image, using equations similar to (32) and (33). We found that $V_{\mathrm{ND}}$ was in fact nonuniform, and that higher values were found in the white matter of the brain. This was a reasonable result, since the nondisplaceable binding is affected by tissue lipophilicity, and the myelin in white matter increases the lipid content compared to

gray matter. Since the human occupancy analysis for this tracer avoided white matter regions, this regional difference in $V_{ND}$ should not affect our occupancy results.

The second major assumption is that $r$ is uniform across regions, i.e., the drug is in equilibrium between plasma and tissue, so that Eq. (31) holds for all regions. This assumption may be invalid if the plasma concentration of drug is changing rapidly, in the time scale of the PET experiment, which is most likely to occur in the early phase post-dosing, especially for drugs with poor tissue penetration. Such an effect can be evaluated by comparing occupancy at early and late times post-dosing at matched plasma levels (Salinas et al. 2013), to assess the presence of pharmacological hysteresis. An example of hysteresis in a human occupancy study was found for a norepinephrine transporter drug (Smith edt al. 2015). More sophisticated models are being developed to account for the dynamics of drug entry into tissue (Abanades et al. 2011).

Nonuniform occupancy across regions could also occur if there are other competing endogenous molecules, which occupy the target protein. The presence of such a molecule would alter the interpretation of the relationship of drug level to occupancy in Eq. (31). By competing with an endogenous compound, the effective $IC_{50}$ (or $K_d$) would be increased. Thus, if the concentration of an endogenous molecule varies across regions, the $IC_{50}$ will vary, as will $r$.

Testing of these assumptions requires more extensive datasets than are conventionally acquired. One approach would be to use occupancy data from multiple subjects, with a global maximum likelihood analysis. Then, a likelihood ratio test could be used to assess if a model that violates the conventional assumption (e.g., nonuniform $V_{ND}$) produces a statistically better fit to the global data than the simpler conventional model. Of course, such a multi-subject model would have to properly account for intersubject variation in drug pharmacokinetics and other sources of between-subject variance.

## 7 Summary and Conclusions

PET imaging is an important quantitative imaging tool in drug development, which has been successfully used to relate drug exposure to target occupancy. The methodology commonly applied is based on sub-optimal statistics; this has developed in part for ease of use. Here, we present maximum likelihood versions of these occupancy methods, for situations with single-subject data in cases where a baseline (no-drug) scan is available and where there is no reference region devoid of the receptor.

Simulation studies showed that the occupancy plot (OCCPLOT) provides similar estimates to the maximum likelihood method based on ordinary least squares (ML-OLS), using typical noise levels seen in regional time-activity curves. If the noise in the $V_T$ estimates is known, our simulation studies showed the variability of occupancy estimates could be lowered by using weighted least squares (ML-WLS), or the full covariance matrix (ML-FCM) when noise in the input function is high. This improvement was most striking for low occupancy cases.

These methods were then applied to 3 human occupancy studies. Using the estimate of input function noise based on test/retest data, ML-WLS and ML-FCM results were very similar. The patterns of higher noise for OCCPLOT and ML-OLS found in the

simulation were not evident in the real-data cases shown. This may be due to the small number of data points per study and/or to violations of the assumptions of the ML methods.

The newly proposed methods are likely to be most useful, i.e., to reduce bias and variability, in cases where (1) there is variation in the data variance between regions, (2) there is high noise in the input function determination producing global variability in $V_{T,}$ and poor test/retest variability (such as with $^{11}$C–PK11195 or $^{11}$C–WAY100635), and (3) occupancy is low. As with any approach, inconsistencies between the assumptions of the method and the real data can cause poorer performance than that found in simulations, where all the assumptions can be met. Thus, best use of these approaches with real data will be realized by improving the accuracy of the data covariance matrix.

These approaches can naturally adapt to other scenarios (reference region present and no baseline scan available) and can be used for estimation of $IC_{50}$ from individual or group data. We expect that application of these methods based on maximum likelihood in future PET occupancy studies will both improve the precision of PET results and allow more comprehensive testing of the assumptions inherent in these analyses.

## References


Abanades S et al (2011) Prediction of repeat-dose occupancy from single-dose data: characterisation of the relationship between plasma pharmacokinetics and brain target occupancy. J Cereb Blood Flow Metab 31:944–952. https://doi.org/10.1038/jcbfm.2010.175

Carson RE (2000) PET physiological measurements using constant infusion. Nucl Med Biol 27:657–660

Carson RE (2003) Tracer kinetic modeling. In: Valk PE, Bailey DL, Townsend DW, Maisey MN (eds) Positron emission tomography: basic science and clinical practice. Springer, London, pp 147–179

Carson RE, Channing MA, Blasberg RG, Dunn BB, Cohen RM, Rice KC, Herscovitch P (1993) Comparison of bolus and infusion methods for receptor quantitation: application to [18F]cyclofoxy and positron emission tomography. J Cereb Blood Flow Metab 13:24–42. https://doi.org/10.1038/jcbfm.1993.6

Castner SA et al (2014) Relationship between glycine transporter 1 inhibition as measured with positron emission tomography and changes in cognitive performances in nonhuman primates. Neuropsychopharmacology. https://doi.org/10.1038/npp.2014.4

Chen KW, Huang SC, Yu DC (1991) The effects of measurement errors in the plasma radioactivity curve on parameter estimation in positron emission tomography. Phys Med Biol 36:1183–1200

Cobelli C, Foster D, Toffolo G (2001) Tracer kinetics in biomedical research: from data to model. Plenum Publishing, New York

Cosgrove KP et al (2011) Assessing the sensitivity of [(1)(1)C]p943, a novel 5-HT1B radioligand, to endogenous serotonin release. Synapse 65:1113–1117. https://doi.org/10.1002/syn.20942

Cunningham VJ, Rabiner EA, Slifstein M, Laruelle M, Gunn RN (2010) Measuring drug occupancy in the absence of a reference region: the Lassen plot re-visited. J Cereb Blood Flow Metab 30:46–50. https://doi.org/10.1038/jcbfm.2009.190

DiMasi JA, Hansen RW, Grabowski HG (2003) The price of innovation: new estimates of drug development costs. J Health Econ 22:151–185

Esterlis I et al (2013) Imaging changes in synaptic acetylcholine availability in living human subjects. J Nucl Med 54:78–82. https://doi.org/10.2967/jnumed.112.111922

Finnema SJ et al (2016) Imaging synaptic density in the living human brain. Sci Transl Med 8:348–396

Gallezot JD et al (2011) Evaluation of [(11)C]MRB for assessment of occupancy of norepinephrine transporters: Studies with atomoxetine in non-human primates. NeuroImage 56:268–279. https://doi.org/10.1016/j.neuroimage.2010.09.040

Gallezot JD et al (2012) Affinity and selectivity of [(1)(1)C]-(+)-PHNO for the D3 and D2 receptors in the rhesus monkey brain in vivo. Synapse 66:489–500. https://doi.org/10.1002/syn.21535

Gallezot JD et al (2017) Determination of receptor occupancy in the presence of mass dose: [11C]GSK189254 PET imaging of histamine H3 receptor occupancy by PF-03654746. J Cereb Blood Flow Metab 37:1095–1107. https://doi.org/10.1177/0271678x16650697

Gunn RN, Gunn SR, Cunningham VJ (2001) Positron emission tomography compartmental models. J Cereb Blood Flow Metab 21:635–652. https://doi.org/10.1097/00004647-200106000-00002

Hillmer AT et al (2016) PET imaging evaluation of [(18)F]DBT-10, a novel radioligand specific to alpha7 nicotinic acetylcholine receptors, in nonhuman primates. Eur J Nucl Med Mol Imaging 43:537–547. https://doi.org/10.1007/s00259-015-3209-0

Huesman RH, Mazoyer BM (1987) Kinetic data analysis with a noisy input function. Phys Med Biol 32:1569–1579

Ichise M et al (2003) Linearized reference tissue parametric imaging methods: application to [$^{11}$C]DASB positron emission tomography studies of the serotonin transporter in human brain. J Cereb Blood Flow Metab 23:1096–1112. https://doi.org/10.1097/01.WCB.0000085441.37552.CA

Ichise M, Toyama H, Innis RB, Carson RE (2002) Strategies to improve neuroreceptor parameter estimation by linear regression analysis. J Cereb Blood Flow Metab 22:1271–1281. https://doi.org/10.1097/00004647-200210000-00015

Innis RB et al (2007) Consensus nomenclature for in vivo imaging of reversibly binding radioligands. J Cereb Blood Flow Metab 27:1533–1539. https://doi.org/10.1038/sj.jcbfm.9600493

Jacquez JA (1985) Compartmental analysis in biology and medicine, 2nd edn. University of Michigan Press, Ann Arbor

Joshi AD et al (2015) Characterization of the novel GlyT1 PET tracer [18F]MK-6577 in humans. Synapse 69:33–40. https://doi.org/10.1002/syn.21782

Kim SJ et al (2013) Determination of the in vivo selectivity of a new kappa-opioid receptor antagonist PET tracer 11C-LY2795050 in the rhesus monkey. J Nucl Med 54:1668–1674. https://doi.org/10.2967/jnumed.112.118877

Lammertsma AA, Hume SP (1996) Simplified reference tissue model for PET receptor studies. Neuroimage 4:153–158. https://doi.org/10.1006/nimg.1996.0066

Li R, Barton HA, Yates PD, Ghosh A, Wolford AC, Riccardi KA, Maurer TS (2014) A "middle-out" approach to human pharmacokinetic predictions for OATP substrates using physiologically-based pharmacokinetic modeling. J Pharmacokinet Pharmacodyn 41:197–209. https://doi.org/10.1007/s10928-014-9357-1

Logan J et al (1990a) Graphical analysis of reversible radioligand binding from time-activity measurements applied to [N-11C-methyl]-(-)-cocaine PET studies in human subjects. J Cereb Blood Flow Metab 10:740–747. https://doi.org/10.1038/jcbfm.1990.127

Logan J et al (1990b) Graphical analysis of reversible radioligand binding from time-activity measurements applied to [N-11C-methyl]-(-)-cocaine PET studies in human subjects. J Cereb Blood Flow Metab 10:740–747. https://doi.org/10.1038/jcbfm.1990.127

Logan J, Fowler JS, Volkow ND, Wang GJ, Ding YS, Alexoff DL (1996) Distribution volume ratios without blood sampling from graphical analysis of PET data. J Cereb Blood Flow Metab 16:834–840. https://doi.org/10.1097/00004647-199609000-00008

Nabulsi NB et al (2016) Synthesis and preclinical evaluation of 11C-UCB-J as a PET tracer for imaging the synaptic vesicle glycoprotein 2A in the brain. J Nucl Med 57:777–784. https://doi.org/10.2967/jnumed.115.168179

Nabulsi NB, Zheng MQ, Ropchan J, Labaree D, Ding YS, Blumberg L, Huang Y (2011) [$^{11}$C]GR103545: novel one-pot radiosynthesis with high specific activity. Nucl Med Biol 38:215–221. https://doi.org/10.1016/j.nucmedbio.2010.08.014

Naganawa M et al (2014) Evaluation of the agonist PET radioligand [(1)(1)C]GR103545 to image kappa opioid receptor in humans: kinetic model selection, test-retest reproducibility and receptor occupancy by the antagonist PF-04455242. NeuroImage 99:69–79. https://doi.org/10.1016/j.neuroimage.2014.05.033

Naganawa M et al (2015) Test–retest reproducibility of binding parameters in humans with $^{11}$C-LY2795050, an antagonist PET radiotracer for the kappa opioid receptor. J Nucl Med 56:243–248. https://doi.org/10.2967/jnumed.114.147975

Naganawa M et al (2016) Receptor occupancy of the kappa-opioid antagonist LY2456302 measured with positron emission tomography and the novel radiotracer 11C-LY2795050. J Pharmacol Exp Ther 356:260–266. https://doi.org/10.1124/jpet.115.229278

Nicolas JM et al (2016) Brivaracetam, a selective high-affinity synaptic vesicle protein 2A (SV2A) ligand with preclinical evidence of high brain permeability and fast onset of action. Epilepsia 57:201–209. https://doi.org/10.1111/epi.13267

Normandin MD et al (2015) Imaging the cannabinoid CB1 receptor in humans with [11C]OMAR: assessment of kinetic analysis methods, test–retest reproducibility, and gender differences. J Cereb Blood Flow Metab 35:1313–1322. https://doi.org/10.1038/jcbfm.2015.46

Normandin MD, Koeppe RA, Morris ED (2012) Selection of weighting factors for quantification of PET radioligand binding using simplified reference tissue models with noisy input functions. Phys Med Biol 57:609–629. https://doi.org/10.1088/0031-9155/57/3/609

Ogden RT (2003) Estimation of kinetic parameters in graphical analysis of PET imaging data. Stat Med 22:3557–3568. https://doi.org/10.1002/sim.1562

Park E et al (2015) Test-retest reproducibility of the metabotropic glutamate receptor 5 ligand [(18)F]FPEB with bolus plus constant infusion in humans. Eur J Nucl Med Mol Imaging 42:1530–1541. https://doi.org/10.1007/s00259-015-3094-6

Patlak CS, Blasberg RG, Fenstermacher JD (1983) Graphical evaluation of blood-to-brain transfer constants from multiple-time uptake data. J Cereb Blood Flow Metab 3:1–7. https://doi.org/10.1038/jcbfm.1983.1

Salinas C et al (2013) Kinetic analysis of drug-target interactions with PET for characterization of pharmacological hysteresis. J Cereb Blood Flow Metab 33:700–707. https://doi.org/10.1038/jcbfm.2012.208

Saricicek A et al (2015) Test–retest reliability of the novel 5-HT1B receptor PET radioligand [11C]P943. Eur J Nucl Med Mol Imaging 42:468–477. https://doi.org/10.1007/s00259-014-2958-5

Sawant-Basak A et al (2017) Quantitative projection of human brain penetration of the H3 antagonist PF-03654746 by integrating rat-derived brain partitioning and PET receptor occupancy. Xenobiotica 47:119–126. https://doi.org/10.3109/00498254.2016.1166531

Slifstein M, Laruelle M (2000) Effects of statistical noise on graphic analysis of PET neuroreceptor studies. J Nucl Med 41:2083–2088

Smith JA et al (2015) Preclinical to clinical translation of CNS transporter occupancy of TD-9855, a novel norepinephrine and serotonin reuptake inhibitor. Int J Neuropsychopharmacol. https://doi.org/10.1093/ijnp/pyu027

Talbot PS et al (2005) $^{11}$C-GR103545, a radiotracer for imaging kappa-opioid receptors in vivo with PET: synthesis and evaluation in baboons. J Nucl Med 46:484–494

Xia Y et al (2015) Measurement of Bmax and Kd with the glycine transporter 1 radiotracer (1)(8)F-MK6577 using a novel multi-infusion paradigm. J Cereb Blood Flow Metab 35:2001–2009. https://doi.org/10.1038/jcbfm.2015.163

Yaqub M, Boellaard R, Kropholler MA, Lammertsma AA (2006) Optimization algorithms and weighting factors for analysis of dynamic PET studies. Phys Med Biol 51:4217–4232. https://doi.org/10.1088/0031-9155/51/17/007